Research Square

Preprints are preliminary reports that have not undergone peer review.
They should not be considered conclusive, used to inform clinical practice,
or referenced by the media as validated information.

Friction-Based Stabilization for Sustainable Temporary Urban Installations and Adaptive Land Use

Muhammad Naqash
Islamic University of Madinah
Antonio Formisano
antoform@unina.it
University of Naples Federico II

Research Article

Keywords: temporary urbanism, adaptive land use, circular construction, urban resilience, reversible architecture, friction-based stabilization, frictional stability index, non-anchored structures

Posted Date: November 18th, 2026

DOI: https://doi.org/10.21203/rs.3.rs-11526539/v1

License: This work is licensed under a Creative Commons Attribution 4.0 International License.
Read Full License

Additional Declarations: No competing interests reported.

Friction-Based Stabilization for Sustainable Temporary Urban Installations and Adaptive Land Use

Muhammad Tayyab Naqash[1], Antonio Formisano[2,*]

[1] Department of Civil Engineering, Islamic University of Madinah, Madinah, Saudi Arabia
[2] Department of Structures for Engineering and Architecture, University of Naples Federico II, Naples, Italy
* Correspondence: antoform@unina.it

Abstract. Exhibition pavilions, pop-up retail units, emergency shelters and event structures make flexible, reversible land use possible, yet the usual way of holding them in place, mechanical anchoring to the floor, damages the host surface, generates waste and adds embodied carbon. This paper develops a friction-based stabilization framework for temporary structures that cannot be anchored. The Frictional Stability Index (FSI), defined as the ratio of base friction capacity to lateral demand, is placed in a design context and extended to a family of indices that account for overturning, amplification of the base shear by a flexible frame, resonance under crowd loading and loss of normal force under vertical floor vibration. A dynamic model of a freestanding booth, combining Coulomb–Stribeck friction, a flexible frame and horizontal and vertical floor motion, is solved in COMSOL Multiphysics for 143 cases and verified against closed-form solutions and the energy balance. Four results stand out: (i) a higher friction coefficient improves stability only until the booth tips rather than slides; (ii) a flexible frame amplifies the base shear by a factor of 1.54 under a 0.6 s floor pulse, so slip begins at a friction coefficient 1.54 times the floor acceleration expressed in g; (iii) slip under crowd loading is confined to a band of roughly ±5 % around the frame frequency; and (iv) creep under a constant lateral load begins once the minimum normal force can no longer carry it, so a static index of 1.5 tolerates vertical floor accelerations up to 0.33 g whereas an index of 1.2 tolerates only 0.17 g. Three exhibition booths analysed as case studies return static indices between 9.5 and 19, and a seismic example shows that the lower-bound design force of ASCE 7-22 can erase the margin of an index of 1.5.

Keywords: temporary urbanism; adaptive land use; circular construction; urban resilience; reversible architecture; friction-based stabilization; frictional stability index; non-anchored structures

1. Introduction

The building and construction sector is responsible for roughly 37 % of global energy- and process-related CO_2 emissions [1], [2]. Reducing that footprint is usually discussed in terms of permanent buildings, but the temporary works that surround them deserve the same attention. Exhibition pavilions, pop-up retail units, event stages and emergency shelters are erected, dismantled and re-erected many times over their service lives, and every deployment is a chance either to waste material or to keep it in circulation. One recurring obstacle is anchoring. High-end venues frequently forbid mechanical floor anchoring to protect polished marble, power-troweled concrete or specialised carpet systems. Where drilling is permitted, the anchors scar the substrate, call for epoxy grout and post-event remediation, and are usually thrown away afterwards. When anchoring is ruled out, the lateral stability of a temporary structure rests entirely on the friction between its base and the floor.

Engineers have long regarded friction as a secondary and somewhat unreliable form of resistance. In a non-anchored system it becomes the primary load path, and it is far from a fixed quantity: the coefficient of friction depends on the material pair, on dust, moisture and wear, and on the condition of the surface, and it scatters considerably in practice [3]. Freestanding contents and nonstructural elements are also known to be vulnerable in earthquakes; post-event surveys repeatedly find unanchored contents damaged more severely than the structural frame that houses

them [4], [5]. The stability of freestanding installations therefore needs to be assessed with a rational, quantitative criterion that designers, venue operators and approving authorities can all check.

This paper proposes such a criterion and examines how far it can be trusted. The Frictional Stability Index (FSI) is the ratio of the friction capacity of the base interface to the horizontal demand (Figure 1). Sliding is prevented when the friction force μN exceeds the horizontal demand F_h, and the index is

$$FSI = \mu N / F_h \quad (1)$$

where μ is the static coefficient of friction and N the normal force. The expression is nothing more than the classical factor of safety against sliding. What is new is not the ratio itself but its adoption as a design and verification parameter for non-anchored temporary structures, together with a systematic examination of when the static ratio is, and is not, sufficient. Values above unity indicate sliding resistance; a higher threshold of 1.5 is adopted here to cover uncertainty in both the friction coefficient and the demand.

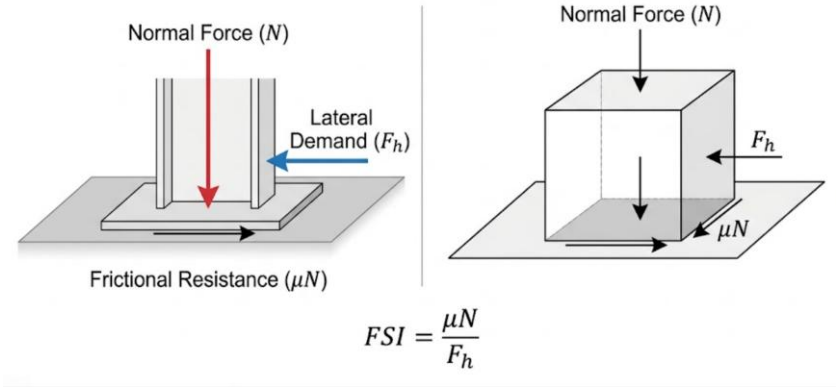


Figure 1. Frictional resistance mechanism at the base interface.

A static ratio has limitations that matter for freestanding booths. A tall or narrow booth may tip before it slides, and once that happens a higher friction coefficient brings no benefit. A flexible frame amplifies the base shear when the floor moves. A crowd can excite the frame close to its natural frequency. Vertical vibration of the floor reduces the normal force during part of each cycle, and the kinetic friction that governs after breakaway is lower than the static value. To capture these effects the paper adds a dynamic model of a freestanding booth, solved in COMSOL Multiphysics for 143 parametric cases.

The contributions are fivefold: (1) a design framework for friction-based stabilization in which the FSI is extended to a family of indices covering overturning, floor-pulse amplification, crowd resonance and creep under vertical vibration; (2) a verified dynamic model and a parametric study that locate the thresholds at which sliding, resonant slip and creep begin; (3) a mapping of these indices onto ASCE 7-22, Eurocode 3 and the Saudi Building Code (SBC 301) [6], including the observation that the lower-bound seismic force can govern the design; (4) three case studies of exhibition booths and a seismic example; and (5) a practical implementation workflow and a discussion of the sustainability and land-use implications. The verification is numerical; no

physical tests were performed, and the results should be calibrated against tests of the actual interface before they are used as design values.

The paper is organised as follows. Section 2 reviews the literature and the relevant codes. Section 3 sets out the static framework; Section 4 presents the dynamic model, its numerical implementation and its verification; and Section 5 reports the parametric results. Section 6 applies the framework to three booths and a seismic example, and Section 7 turns the results into a design workflow. Section 8 discusses sustainability and land use, Section 9 the limitations, and Section 10 draws the conclusions.

2. Literature Review

2.1 Friction as the primary stabilizing mechanism

The design philosophy for temporary structures has shifted from experience-based practice toward analytically verified performance frameworks. Scaffolding, formwork and exhibition booths are more prone to lateral instability than permanent buildings because of their slender members, semi-rigid connections and reliance on base-interface behaviour, and the expectation that temporary installations reach safety levels comparable to permanent ones is now widely shared [7]. Experimental characterisation of scaffold connections gives rotational stiffnesses of 30–40 kN·m/rad, typical of semi-rigid joints [8]; the global stability of such systems depends on how joint flexibility interacts with the frictional resistance at the support, which is precisely the interface examined here.

The friction available at a base depends on the coefficient μ of the contact pair and on the normal force. Typical static coefficients on concrete are 0.3–0.5 for plywood, 0.4–0.6 for aluminium, 0.3–0.6 for steel with an ordinary construction finish, 0.6–0.9 for roughened or treated steel and 0.7–1.0 for rubber (Figure 2). Because the values depend on the test method (EN 13893 [9] for floor coverings, for example), on roughness and on environmental conditions, these ranges are indicative only; polished interfaces may offer μ of just 0.2–0.4. Since the resistance scales directly with μ, the choice of interface material is the first design variable of any non-anchored system.

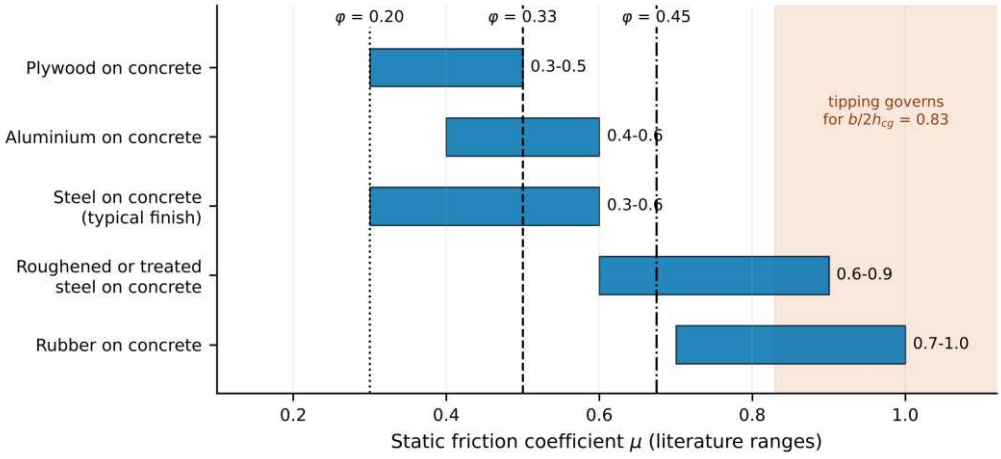


Figure 2. Ranges of the static friction coefficient for common base interfaces on concrete (literature values quoted in the text). The vertical lines mark the friction coefficient required for FSI = 1.5 at demand ratios $\varphi = F_h/W$ of 0.20, 0.33 and 0.45; the shaded zone is the range in which a booth with $b/2h_{cg} = 0.83$ tips instead of sliding (Section 3.2).

Static friction governs the onset of sliding, whereas the lower kinetic friction governs what happens afterwards: a structure that has begun to slide will continue to move under a smaller force. Design must therefore prevent slip initiation rather than rely on post-sliding behaviour. Roughening, texturing and coatings are established means of raising friction [10], [11]; rubber pads add both friction and damping, although the long-term behaviour of rubber–metal interfaces under cyclic load, wear and ageing requires attention [3], [12]. Friction enhancement should therefore be embedded in a performance-based procedure rather than applied as an empirical afterthought. Degradation of a design parameter by pollution or wear can be expressed through a modifier, as has been proposed for aluminium façades [13]; an analogous modifier on μ is a natural extension of the present framework.

Friction-based stabilization also sits comfortably within the aims of circular construction. The built environment accounts for about half of the material extracted in the European Union and for more than a third of its waste [14], and the lack of sector-specific standards limits the uptake of design for manufacture and assembly and of design for deconstruction [15]. A stabilization method that leaves no trace in the floor and allows every component to be reused addresses both concerns, but only if its safety can be demonstrated in a form that authorities will accept.

2.2 Dynamic and seismic vulnerability

Exhibition booths frequently behave as single-degree-of-freedom systems whose stability hinges on their dynamic response. Walking and running excite frequencies of 1.5–2.5 Hz, and synchronised activity such as dancing or rhythmic clapping can reach 3.5 Hz [16], [17]. A booth whose natural frequency lies near this range is exposed to resonance. Friction at the base introduces nonlinear damping: it caps the force that can be transmitted to the frame, at the price of slip, and in doing so changes the response qualitatively. Human–structure interaction further adds mass, stiffness and damping to the structure and can shift natural frequencies, with consequences for resonance and for tuned control devices [18]–[20].

The response of unanchored freestanding bodies to earthquakes is governed by rigid-body motion, mainly sliding and rocking, and depends on slenderness and on the roughness of the base [21]. Incremental dynamic analyses of rigid blocks under ground and floor motions show that acceleration- and velocity-based parameters control overturning and that shake-table protocols do not always give conservative estimates of the response to real motions [22]. The criteria that decide whether a rigid block slides, rocks or does both are classical [23]–[25], and the sliding-block model of Newmark [26] gives the permanent displacement under a given acceleration pulse; both are used for verification in Section 4. Base isolation reduces drift and acceleration but not necessarily floor velocity, so velocity-sensitive freestanding contents can be at greater risk in isolated buildings [5]; friction-based resistance at the level of the contents, by contrast, does not depend on the building system. Reviews of seismic isolation and energy dissipation describe the state of the art of sliding and elastomeric systems [27], [28], and the review of rocking-dominated nonstructural elements underlines the need for fragility models of freestanding objects [4].

Urban resilience scholarship, for its part, calls for measurable performance indicators that connect engineering decisions to the adaptive capacity of cities [29]–[31]. By casting stabilization as a capacity–demand ratio, the FSI supplies such an indicator at the scale of the individual installation.

2.3 Codes and standards

ASCE 7-22 [32] specifies the lateral force on nonstructural components (Section 13.3; Eq. (5) below) and requires a component importance factor I_p of 1.5 for components that must remain functional for life safety after an earthquake, such as egress stairways. Section 13.4 requires attachments to be positively fastened, with no credit for the friction produced by gravity. Friction-only verification therefore lies outside the prescriptive path of ASCE 7; where anchorage is prohibited, it can be offered only as a performance-based alternative that the authority having jurisdiction must accept. That is the position taken here: the paper does not claim that the FSI satisfies the prescriptive requirement.

Eurocode 3, Part 1-8 [33], recognises friction only in slip-resistant bolted connections and offers no provisions for the friction of an unanchored base on a floor. The Saudi Building Code (SBC 301) [34] is based on the International Building Code and ASCE 7, with Saudi-specific wind and seismic parameters, and requires structures to maintain integrity and serviceability under all load combinations. A safety factor of 1.5 against sliding and overturning is customary in geotechnical design, for instance for retaining walls in the International Building Code [35]; this convention, together with the variability of μ examined in Section 3.4, underpins the target index of 1.5 adopted here. The target is not derived from the importance factor I_p, which enters the demand through the seismic force rather than the threshold. Table 1 summarises the position of each code.

Table 1. Codes and standards considered and their relation to friction-based stabilization.

Code or standard	Relevant provisions	Consequence for non-anchored booths
ASCE 7-22	Seismic force on nonstructural components (13.3); $I_p = 1.5$ for life-safety components; positive attachment (13.4)	Friction-only verification is a performance-based alternative that needs acceptance by the authority
IBC 2021	General structural integrity; safety factor 1.5 against sliding and overturning for retaining walls	Supports a target index of 1.5
Eurocode 3 (EN 1993-1-8)	Friction only in slip-resistant bolted joints	No provisions for floor friction; additional factors required
SBC 301	Loads and forces, based on IBC and ASCE 7	Local wind and seismic parameters; same alternative route

2.4 Research gap and positioning

Table 2 sets out the strengths, weaknesses, opportunities and threats of the approach and places the proposed framework in context. Despite the extensive literature on rocking blocks, friction models and nonstructural elements, no friction-based performance index with verified failure thresholds exists for temporary installations operating under venue restrictions on anchoring. The present study closes that gap in three steps: it defines the index and its extensions, verifies the thresholds numerically, and shows how the index enters design practice and sustainability assessment.

Table 2. Assessment of friction-based stabilization.

Strengths	Weaknesses
Damage-free installation; reusable components; no anchor waste; a single quantitative index that fits code workflows	Sensitive to the friction coefficient; dependent on surface cleanliness; limited field validation
Opportunities	Threats
Smart or textured interface materials; monitoring of stability; integration with circular-construction practice	Conservative code interpretation; misapplication without checking the governing demand; contamination of the floor

3. Static Framework

3.1 Frictional Stability Index

Equation (1) is evaluated with N taken as the sum of the vertical reactions of the structure under the governing load combination; for seismic or dynamic combinations N is the minimum compressive reaction and F_h the corresponding horizontal reaction. The proposed classification is FSI > 1.5 stable (the recommended design level), $1.0 \leq FSI \leq 1.5$ marginal, requiring monitoring or interface modification, and FSI < 1.0 unstable. The workflow of Figure 21 in Section 7 shows how the index is used in practice. If the index falls below 1.5, the design is changed by adding ballast or by raising the interface friction through material substitution or surface treatment.

3.2 Overturning and the failure mode

A non-anchored booth must also resist overturning. With W the weight, b the base width in the direction of the load and h_{cg} the height of the centre of gravity, the restoring moment is Wb/2 and the overturning moment is $F_h h_{cg}$. Writing $\varphi = F_h/W$ for the horizontal demand as a fraction of the weight, the overturning index and the combined index are

$$FSI_o = (W\ b/2) / (F_h\ h_{cg}) = (b/2h_{cg}) / \varphi \tag{2}$$

$$FSI_{eff} = \min(FSI_s, FSI_o) = \min(\mu, b/2h_{cg}) / \varphi \tag{3}$$

where FSI_s is the sliding index of Eq. (1). The two modes exchange at

$$\mu^* = b / 2h_{cg} \tag{4}$$

Above μ^* a higher friction coefficient no longer raises the index, because the booth tips instead of sliding [23]–[25]. For a booth with $b/2h_{cg} = 0.6$ and $\varphi = 1/3$, raising μ from 0.3 to 0.9 lifts the combined index from 0.9 to 1.8, not from 0.9 to 2.7 as the sliding-only index would suggest. Figure 3a illustrates the effect for $\varphi = 0.25$, and Figure 3b maps the failure mode in the plane of friction coefficient and slenderness. The familiar statement that higher friction always improves stability therefore holds only for $\mu < \mu^*$.

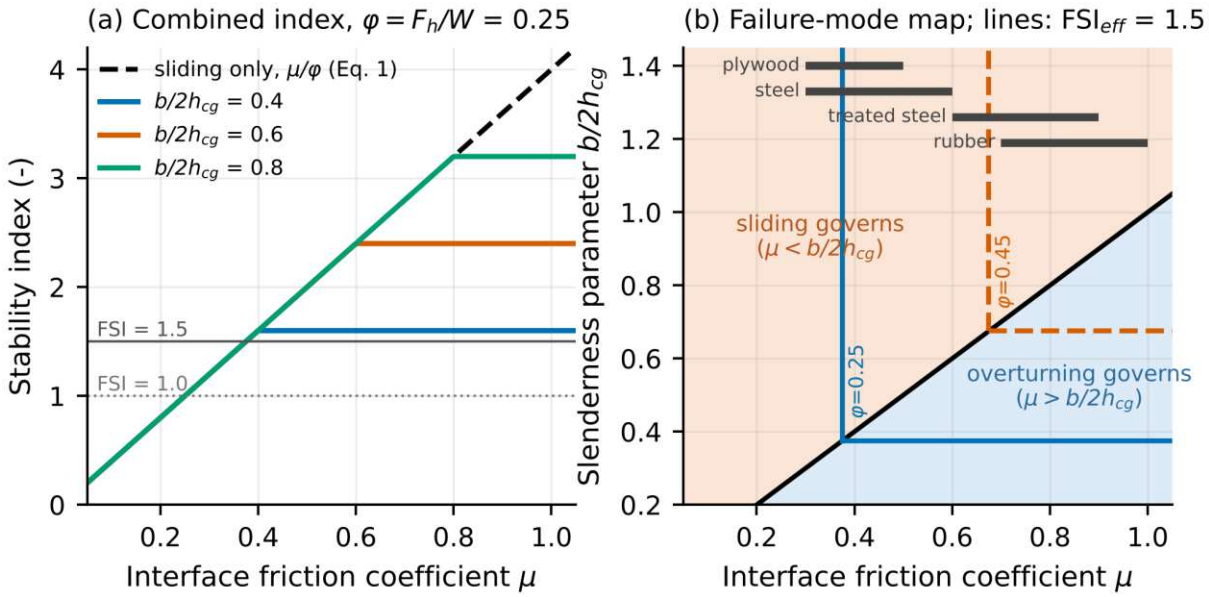


Figure 3. (a) Combined sliding/overturning index against the friction coefficient for φ = 0.25; (b) failure-mode map in the plane of friction coefficient and slenderness, with the lines FSI_{eff} = 1.5 for φ = 0.25 and for φ = 0.45 (the lower-bound seismic force of Section 6.2). The bars show the friction ranges of Figure 2.

3.3 Seismic demand

For a nonstructural component the seismic force of ASCE 7-22 [32] is

$$F_p = 0.4\, S_{DS}\, I_p\, W_p\, (H_f/R_\mu)\, (C_{AR}/R_{po}) \tag{5}$$

$$0.3\, S_{DS}\, I_p\, W_p \le F_p \le 1.6\, S_{DS}\, I_p\, W_p \tag{6}$$

where S_{DS} is the design spectral acceleration at short periods (in g), W_p the operating weight of the component, H_f the height amplification factor, R_μ the structure ductility reduction factor, C_{AR} the component resonance amplification factor and R_{po} the component strength factor. At the base level H_f = 1. The lower bound of Eq. (6) governs whenever $H_f C_{AR}/R_\mu R_{po} < 0.75$, which is the usual situation for a rigid component at floor level (C_{AR} = 1.0, $R_\mu \ge 1$, $R_{po} \ge 1.5$); a flexible booth with $C_{AR} > 1$ must be checked separately. The equation of the 2016 edition, $F_p = 0.4 a_p S_{DS} W_p (1 + 2z/h)/(R_p/I_p)$, gives a lower value for the same booth than Eq. (5) and is not used here. The seismic force is incorporated in F_h when the index is evaluated, and Section 6.2 shows that the choice of equation changes the verdict.

3.4 Variability of the friction coefficient

Because the friction coefficient varies with surface condition, tolerances and degradation, it can be treated as a random variable, $\mu \sim N(\bar{\mu}, \sigma)$. Sliding occurs when μ falls below the critical value $\mu_c = F_h/N = \varphi$, and the probability of sliding is

$$P_{slide} = \Phi[(\mu_c - \bar{\mu}) / \sigma] \tag{7}$$

where Φ is the standard normal distribution function. With $\mu_c = \bar{\mu}/FSI_{design}$, the probability is tied directly to the design index. For $\bar{\mu}$ = 0.5 and σ = 0.10, an index of 1.5 corresponds to a probability of sliding of 4.8 %, and an index of 1.2 to 20.2 %. This calibration shows that the target of 1.5 offers meaningful robustness against realistic friction variability; Section 5.7 extends the argument to vertical floor vibration.

4. Dynamic Model and Numerical Method

4.1 Why a numerical model is needed

The static index of Eq. (1) is exact for a rigid body pushed slowly by a known horizontal force, and the verification in Section 4.4 confirms that slip begins when FSI = 1. A freestanding booth departs from this idealisation in three ways. First, the combined index of Section 3.2 shows that the failure mode may switch from sliding to tipping. Second, the force that reaches the interface is not the applied force: a flexible frame amplifies the base shear under dynamic excitation, while friction itself caps the force the frame can transmit. Third, the normal force is not constant, since vertical floor vibration reduces it during part of each cycle, and kinetic friction is lower than static friction [36], [37]. The last two effects can only be resolved with a dynamic model.

4.2 Formulation

The booth is idealised as three parts (Figure 4): an upper mass m (frame and contents), a small base mass m_b (base plates and base frame) that rests on the floor, and a lateral frame stiffness k and damping c connecting them. The floor can move horizontally with acceleration $a_g(t)$ and vertically with acceleration $a_v(t)$, and a horizontal force F(t) acts on the upper mass. Two displacements describe the response: the slip s of the base on the floor and the drift u of the upper mass relative to the base. For a freestanding booth the spring belongs to the frame and does not restrain the slip, which distinguishes the system from a single-degree-of-freedom oscillator whose spring is attached to the ground.

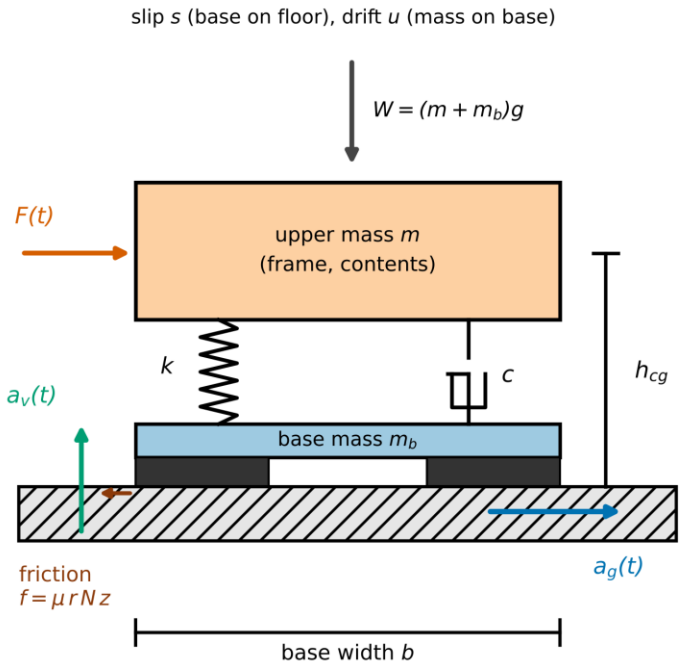


Figure 4. Idealization used in the dynamic model: upper mass m, frame spring k and damper c, base mass m_b, friction at the interface, and the three loads F(t), $a_g(t)$ and $a_v(t)$.

Newton's second law for the two masses gives

$$m(a_g + \ddot{s} + \ddot{u}) + c\,\dot{u} + k\,u = F(t) \tag{8}$$

$$m_b(a_g + \ddot{s}) = c\,\dot{u} + k\,u - f \tag{9}$$

where f is the friction force at the interface. It is described by a Coulomb law with a drop from static to kinetic friction (Stribeck) and a short pre-slip element of the Dahl type [37], [38]:

$$f = \mu\, r_s\, N(t)\, z, \quad r_s = r_k + (1 - r_k)\, e^{-(\dot{s}/v_s)^2\}} \tag{10}$$

$$\dot{z} = (\dot{s} - |\dot{s}|\, z) / \delta, \quad |z| \le 1 \tag{11}$$

Here μ is the static coefficient, r_k the ratio of kinetic to static friction, v_s the Stribeck velocity, z a dimensionless state that equals ±1 during sliding, and δ the pre-slip displacement. The Dahl state replaces the discontinuous sign function with a smooth law, and as $\delta \to 0$ the exact Coulomb solution is recovered, as Section 4.4 demonstrates. The normal force follows the vertical floor acceleration:

$$N(t) = (m + m_b)(g + a_v(t)) \tag{12}$$

The energy balance, used as a check on every run, states that the work of the loads equals the kinetic and elastic energy plus the viscous and frictional dissipation:

$$W_{in} = \int_0^t [(F - m\, a_g)(\dot{s} + \dot{u}) - m_b\, a_g\, \dot{s}]\, d\tau = \tfrac{1}{2}\, m(\dot{s} + \dot{u})^2 + \tfrac{1}{2}\, m_b\, \dot{s}^2 + \tfrac{1}{2}\, k\, u^2 + \int_0^t c\, \dot{u}^2\, d\tau + \int_0^t f\, \dot{s}\, d\tau \tag{13}$$

The loads are a horizontal force with a ramp, a mean and a harmonic part, $F(t) = F_r(t) + F_m + F_0 \sin(2\pi f_F t)$; a rectangular or one-cycle sine pulse of floor acceleration; and a harmonic vertical floor acceleration $a_v(t) = a_{v0}\, g \sin(2\pi f_v t)$. Table 3 lists the reference booth. Its natural frequency of 4 Hz respects the 3.5 Hz limit used in practice to separate a booth from crowd excitation; the stiffness follows from $k = m(2\pi f_n)^2$, the damping from $c = 2\zeta\sqrt{(km)}$, and the quality factor of the frame is $Q = 1/2\zeta$. The height h_{cg} and width b serve only to evaluate the overturning ratio of Eq. (2) and play no part in the sliding model.

Table 3. Parameters of the reference booth and of the friction model.

Parameter	Symbol	Value
Upper mass / base mass	m / m_b	450 kg / 50 kg (total 500 kg, W = 4.905 kN)
Natural frequency, damping ratio	f_n, ζ	4 Hz, 2 % (k = 284 kN/m, Q = 25)
Centre-of-gravity height, base width	h_{cg}, b	1.2 m, 2.0 m ($b/2h_{cg} = 0.83$)
Static friction coefficient	μ	0.1 to 1.0 (varied)
Kinetic / static ratio	r_k	1.0 (0.5 to 1.0 in family 6)
Stribeck velocity, pre-slip displacement	v_s, δ	5 mm/s, 0.005 mm
Gravity	g	9.81 m/s²

4.3 Implementation and case matrix

The model was implemented in COMSOL Multiphysics 5.6 [39] through the Global ODEs and DAEs interface, so that no additional module is required (Figure 5).

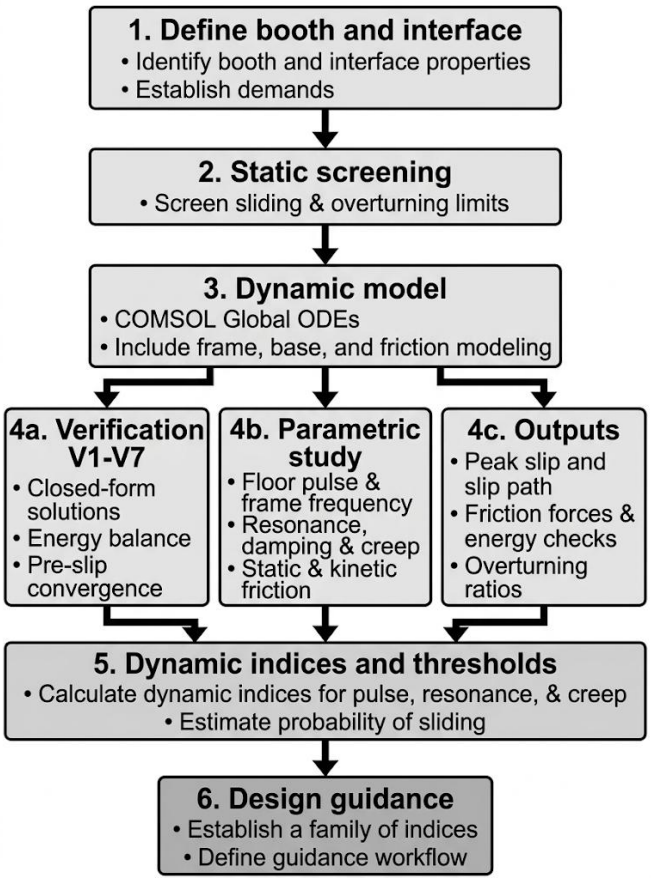
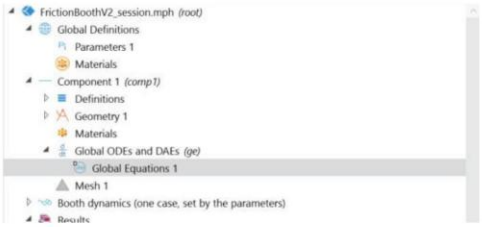


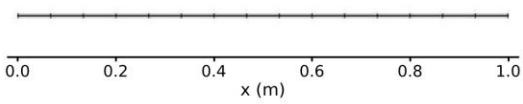
Figure 5. Workflow of the numerical study.

Figure 6 shows the model as it stands in COMSOL. The equations of Section 4.2 describe a lumped system and contain no spatial field, yet a time-dependent study in COMSOL still requires a geometry and a mesh. The component therefore carries a one-dimensional interval of unit length, meshed with the default edge mesh of 15 elements (Figure 6b). Because the unknowns are global quantities that do not vary along the interval, the mesh takes no part in the solution. A zero-dimensional point component would have been the natural choice, but this version of the software did not accept it for the study used here. The physics resides entirely in the Global Equations node of Figure 6c with its 14 states, which Table 4 lists in mathematical form.

(a) Model Builder tree



(b) Carrier geometry and mesh (Mesh 1 selected)



Interval i1 (0 to 1 m): 2 vertices, 1 domain.
Edge mesh edg1, default size: 16 vertices, 15 elements.
The 14 global states do not depend on x; the mesh is required by the study but is not used by the equations.

(c) Global Equations node: the 14 states and their residual equations f = 0 (T0 = 1 s, Lmm = 1000 mm/m)

Name	f(u,ut,utt,t) (1)	Initial value (u_0) (1)	Initial value (u_t0) (1/s)	Description
sl	slt*T0-vsl	0	0	Slip of the base on the floor (mm)
vsl	vslt*T0-acc_b	0	0	Slip velocity (mm/s)
zf	zft*T0-(vsl-abs(vsl)*zf)/dps	0	0	Dahl friction state
xu	xut*T0-wu	0	0	Frame drift (mm)
wu	wut*T0-(Lmm*((Fext-kuc)/mass-ag_t)-...	0	0	Frame drift velocity (mm/s)
Win	Wint*T0-((Fext-mass*ag_t)*(vsl+wu)-...	0	0	Work of the loads (J)
Df	Dft*T0-ffr*vsl/Lmm	0	0	Friction work (J)
Dv	Dvt*T0-cfr*(wu/Lmm)^2	0	0	Viscous dissipation (J)
Path	Patht*T0-abs(vsl)	0	0	Slip path length (mm)
sM	sMt*T0-max(abs(sl)-sM,0)/tauM	0	0	Running maximum of |slip| (mm)
uM	uMt*T0-max(abs(xu)-uM,0)/tauM	0	0	Running maximum of |frame drift| (m...
fM	fMt*T0-max(abs(ffr)-fM,0)/tauM	0	0	Running maximum of |friction force| (...
kM	kMt*T0-max(abs(kuc)-kM,0)/tauM	0	0	Running maximum of |frame force| (N)
Fon	Font*T0-Fr*(1-flc2hs(abs(sl)-1,0.2))	0	0	Force at 1 mm of slip, ramp loading (N)

Figure 6. The booth model in COMSOL Multiphysics 5.6, captured from the saved session model: (a) Model Builder tree with the Global ODEs and DAEs interface; (b) carrier geometry (an interval of unit length) with its default edge mesh of 15 elements, as drawn in the graphics window; (c) the Global Equations node with the 14 states and their residual equations in the notation (sl = s, vsl = v, zf = z, xu = u, wu = w; T0 = 1 s and Lmm = 1000 mm/m carry the units). The geometry and the mesh are required by the study but are not used by the equations.

Five states are physical: the slip s, the slip velocity v, the Dahl state z, the drift u and the drift velocity w. Three further states integrate the energy terms of Eq. (13), one accumulates the slip path length, and five are monitors that record the running maxima of s, u, f and ku + cw together with the force at slip onset. Lengths are carried in millimetres and time in seconds. The equations of Table 4 are Eqs. (8), (9) and (11) solved for the highest derivatives, with $\dot{v}$ taken from Eq. (9) and substituted into Eq. (8). A monitor tracks the peak of its signal with a lag of the order of τ_M = 2 ms and therefore slightly underestimates peaks that last only a few milliseconds; Section 4.4 identifies where this matters. The floor-acceleration pulses are smoothed with a C^2-continuous step function of 2 ms rise time so that the solver always sees continuous loads.

Table 4. States of the COMSOL model and their equations (consistent units; the model carries lengths in mm). H is a smoothed step of 0.2 mm width and F_r the rate of the force ramp.

State	Meaning	Equation
s	Slip of the base	$\dot{s} = v$
v	Slip velocity	$\dot{v} = (ku + cw - f)/m_b - a_g$
z	Dahl state	$\dot{z} = (v - \lvert v\rvert\, z)/\delta$
u	Frame drift	$\dot{u} = w$
w	Drift velocity	$\dot{w} = (F - ku - cw)/m - a_g - \dot{v}$
W_{in}	Work of the loads	$\dot{W}_{in} = (F - m\,a_g)(v + w) - m_b\,a_g\,v$
D_f	Frictional dissipation	$\dot{D}_f = f\,v$

State	Meaning	Equation
D_v	Viscous dissipation	$\dot{D}_v = c\,w^2$
P	Slip path length	$\dot{P} = \lvert v \rvert$
s_M, u_M, f_M, k_M	Running maxima of $\lvert s \rvert$, $\lvert u \rvert$, $\lvert f \rvert$ and $\lvert ku + cw \rvert$	$\dot{M} = \max(\lvert x \rvert - M, 0)/\tau_M$
F_{on}	Force at slip onset	$\dot{F}_{on} = F_r\,[1 - H(\lvert s \rvert - 1\ \text{mm})]$

The system is integrated with the time-dependent BDF solver at a relative tolerance of 10^{-6}, with free steps, an initial step of 10^{-5} s and a maximum step of $\min(0.01\ \text{s}, 0.1/\max(f_n, f_F, f_v))$. Results are stored at 2000 to 4000 equally spaced times per case. The complete run of 143 cases took 12.4 h on the authors' PC. The cases are organised in nine families (Table 5), and the booth parameters of Table 3 apply unless stated otherwise.

Table 5. Case matrix of the parametric study.

Family	Purpose	Varied parameters	Cases
1	Verification V1–V6	slow force ramp; rigid block under a rectangular pulse; resonance without slip; energy balance; pre-slip $\delta = 0.05$ to 0.001 mm	11
2	Floor pulse	$\mu = 0.2$ to $0.9 \times a_g = 0.20$, 0.30, 0.45 g; one-cycle sine, $T_p = 0.6$ s	24
3	Crowd force, frequency sweep	$f/f_n = 0.25$ to 2.0 at $\mu = 0.5$, $F_0/W = 0.04$, 30 s	13
4	Crowd force at resonance	$\mu = 0.1$ to $1.0 \times F_0/W = 0.02$, 0.04; 30 s	16
5	Creep under vertical vibration	$\mu = 0.3$, 0.4, $0.5 \times a_{v0} = 0$ to 0.6 g at 3 Hz; mean load $F_m/W = 0.25$	21
6	Static versus kinetic friction	$\mu_s = 0.4$, $0.6 \times r_k = 1.0$ to 0.5; pulse 0.7 g	8
7	Amplification of the base shear	$f_n = 1$ to 20 Hz × pulse duration 0.3, 0.6, 1.2 s; $a_g = 0.2$ g, $\mu = 1$ (no slip)	27
8	Damping and resonant slip	$\zeta = 0.01$, 0.05, $0.10 \times \mu = 0.1$ to 0.6; $F_0/W = 0.04$; 20 s	15
9	Creep, frequency of the vibration	$f_v = 1$ to 8 Hz with the flexible frame and $f_v = 2$, 3, 8 Hz with a rigid frame ($f_n = 40$ Hz); $\mu = 0.3$, $a_{v0} = 0.25$ g, $F_m/W = 0.25$; 20 s	8

4.4 Verification

Six tests check the implementation against closed-form results (Table 6, Figure 7); a seventh, the response of the frame without friction, is described in Section 5.2. V1 applies a slow force ramp and records the force at which the base has slipped 1 mm. COMSOL returns 2466.3 N, which exceeds $\mu N = 2452.5$ N by 0.6 %, confirming that FSI = 1 of Eq. (1) is the exact slip threshold for

slow loading. V2 and V3 load a rigid block (nearly all the mass placed in the base) with a rectangular floor pulse of amplitude $a_0 = 0.4$ g and duration $T_p = 0.5$ s. The classical sliding-block solution [26] gives the final slip

$$s_{res} = a_0(a_0 - \mu_k g)\, T_p^2 / (2\, \mu_k\, g) \tag{14}$$

with μ_k the kinetic coefficient. Eq. (14) gives 163.5 mm for V2 ($\mu_k = \mu = 0.3$) and 443.8 mm for V3 ($\mu_k = 0.7\ \mu$). COMSOL gives 166.1 mm (+1.6 %) at the default pre-slip length of 0.005 mm and 164.2 mm (+0.4 %) for $\delta = 0.001$ mm (V6), converging monotonically as δ decreases (Figure 7b), and 445.7 mm (+0.4 %) for V3. V4 drives the stuck frame at its natural frequency; the drift amplitude reaches the analytical value of Eq. (15),

$$u_{max} = F_0 / (2\zeta k) = Q\, F_0 / k \tag{15}$$

within 0.02 % (0.8626 mm against 0.8628 mm) and follows the exponential build-up envelope (Figure 7c).

Table 6. Verification of the COMSOL model against closed-form results; the last column gives the difference from the reference.

Test	**Quantity**	**Reference**	**COMSOL**	**COMSOL against reference**
V1	Force at 1 mm slip, N	2452.5 (μN)	2466.3	+0.6 %
V2	Rigid block, residual slip, mm	163.5	166.1	+1.6 %
V3	Same, $r_k = 0.7$, mm	443.8	445.7	+0.4 %
V4	Resonance drift amplitude, mm	0.8628	0.8626	−0.02 %
V5	Energy residual ε_E (sliding, harmonic force)	0	1.4×10^{-6}	–
V6	δ = 0.05 / 0.01 / 0.002 / 0.001 mm, residual slip, mm	163.5	172.8 / 167.5 / 164.8 / 164.2	+5.7 / +2.4 / +0.8 / +0.4 %

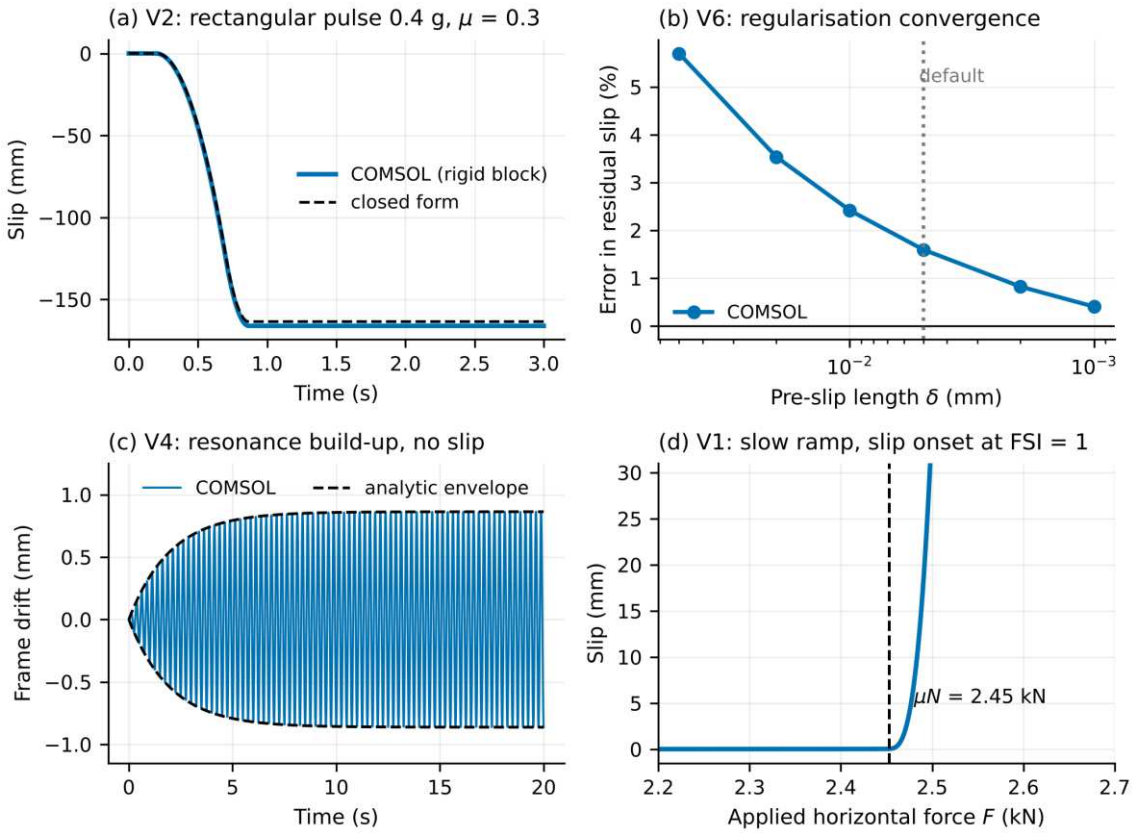


Figure 7. Verification of the COMSOL model: (a) slip history of a rigid block under a rectangular floor pulse against the closed form; (b) error against the pre-slip length δ; (c) resonance build-up of the stuck frame against the analytical envelope; (d) slip against applied force in a slow ramp (V1).

Finally, the energy balance of Eq. (13) is checked in every case through the residual

$$\varepsilon_E = \max_t |W_{in} - (E_k + E_e + D_v + D_f)| \,/\, \max_t W_{in} \tag{16}$$

where W_{in} is the work of the loads, E_k and E_e the kinetic and elastic energy, and D_v and D_f the viscous and frictional dissipation, all taken from the stored solution. COMSOL integrates these energies as additional states at a relative tolerance of 10^{-6}. Over the 143 cases the median residual is 1.1×10^{-5} and the largest value 9.5×10^{-4}, which occurs in case 143 (the rigid frame under a vertical vibration of 8 Hz; Figure 8b). V5, the sliding case with a harmonic force, closes to 1.4×10^{-6} (Figure 8a). The balance therefore closes to a part in a thousand or better in every case, consistent with the solver tolerance.

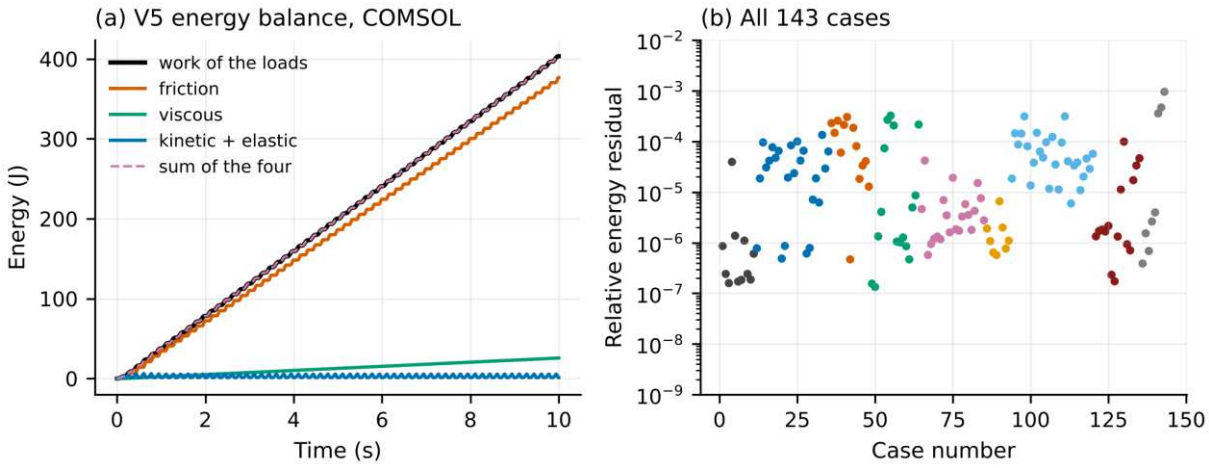


Figure 8. Energy balance of the COMSOL model: (a) V5, the work of the loads against the kinetic and elastic energy and the viscous and frictional dissipation; (b) residual ε_E of Eq. (16) in all 143 cases, coloured by case family.

These checks test the implementation and the numerical settings, not the physical assumptions; the friction law and its parameters still need calibration against tests on real booths, which Section 9 lists as future work. Two numerical points bear on the results that follow. In case 65 ($\mu = 0.3$, no vertical vibration, static index 1.2) the base should remain stuck. COMSOL holds it to a micro-slip of 0.009 mm up to about 7 s, after which the base drifts at roughly 0.02 mm/s to 0.41 mm at 30 s while the Dahl state stays at its stuck value of 5/6. That is not a consistent solution of Eqs. (9) and (11), and we read it as drift of the BDF integrator within its absolute tolerance; it remains below the 1 mm slip criterion. The friction-force monitor also lags the true peak in very short events: in V3 it reads 1287.5 N while the largest stored output point is 1410.6 N. The lag affects only peaks lasting a few milliseconds, such as those of the rigid blocks, and none of the thresholds in Section 5 depends on them.

5. Parametric Results

All results in this section come from the COMSOL runs. Peak values are the end-of-run values of the monitor states, and the curves in Figures 9 to 15 are drawn from the stored time histories of the solved cases. The slip criterion adopted below is a peak slip of 1 mm, comfortably above the micro-slip of the Dahl element (about 0.01 mm).

5.1 Floor pulse

Family 2 subjects the reference booth to a one-cycle sine pulse of floor acceleration lasting 0.6 s. The largest amplitude, 0.45 g, equals the lower-bound seismic force of ASCE 7-22 for this booth with $S_{DS} = 1.0$ g and $I_p = 1.5$ (Section 6.2). Figure 9 conveys three results. First, the peak friction force saturates at the same multiple of the floor acceleration for every amplitude, 1.54 $a_g W/g$ (0.309 W, 0.463 W and 0.695 W): for this pulse and this frame frequency, the frame amplifies the base shear by a factor $\Lambda = 1.54$. Second, slip therefore starts at

$$\mu_c \approx \Lambda \, a_g / g \tag{17}$$

that is, at 0.31, 0.46 and 0.69, rather than at a_g/g as the rigid-block criterion would predict. The simulated peak slip crosses 1 mm between $\mu = 0.2$ and 0.3, 0.4 and 0.5, and 0.6 and 0.7 respectively. Third, for $a_g = 0.45$ g the peak slip falls from 82 mm at $\mu = 0.2$ through 42 mm at 0.3,

23 mm at 0.4, 6.8 mm at 0.5 and 3.0 mm at 0.6 to below 0.03 mm at μ ≥ 0.7. The residual slip is not a monotonic indicator because the base can slide back (2.2 mm at μ = 0.2 after a peak of 82 mm), so the peak slip is the quantity that should be reported.

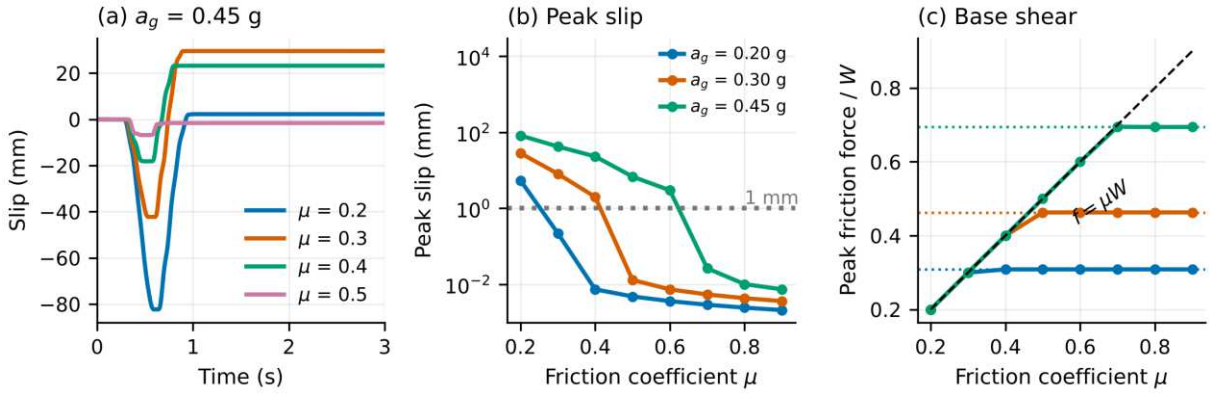


Figure 9. Floor pulse: (a) slip histories at a_g = 0.45 g; (b) peak slip against friction coefficient (dotted line: 1 mm); (c) peak friction force against friction coefficient; the force follows f = μW until it saturates at 1.54 a_gW/g (dotted lines).

5.2 Amplification of the base shear by the frame

The factor Λ = 1.54 of Section 5.1 belongs to one frame frequency (4 Hz) and one pulse duration (0.6 s), and it is not an upper bound. Family 7 isolates the amplification: the booth is held by a friction coefficient of 1 under a one-cycle pulse of 0.2 g so that it does not slip (the peak slip stays below 0.004 mm in all 27 cases), and the frame frequency is varied from 1 to 20 Hz for pulse durations of 0.3, 0.6 and 1.2 s. The amplification factor is defined as the peak friction force divided by a_gW/g.

Figure 10a shows that Λ depends only on the product of frame frequency and pulse duration: the 27 results collapse onto a single curve, and combinations sharing the same product agree within 0.2 % (for example 1.541, 1.543 and 1.544 for f_nT_p = 2.4 obtained with 8 Hz and 0.3 s, 4 Hz and 0.6 s, and 2 Hz and 1.2 s). The amplification peaks at 2.81 when the pulse lasts 1.2 natural periods (f_nT_p = 1.2), drops to 1.54 at f_nT_p = 2.4, the case of the reference booth, and to 1.29 at 3.6, and settles at 1.0–1.1 above 4.8 (Table 7). A very flexible frame with f_nT_p below about 0.5 filters the pulse and transmits less than the rigid-body force (Λ = 0.45 at 0.3). The dashed lines in Figure 10a show the response of the same frame without any friction model, that is, the closed-form response of a linear oscillator on a moving base. The friction model reproduces it in every case, with a median difference of 0.03 % and a largest difference of 0.38 % (the monitor lag again, for the stiffest frame and the shortest pulse). This constitutes the seventh verification test (V7) and checks the stuck phase of the model.

Table 7. Amplification factor Λ of the base shear against the product of frame frequency and pulse duration (frame damping 2 %, one-cycle sine pulse).

f_nT_p	0.3	0.6	0.9	1.2	1.8	2.4	3.6	4.8	7.2
Λ	0.45	1.51	2.48	2.81	1.97	1.54	1.29	1.09	1.12

The practical consequence is that the amplification must be evaluated for the pulse durations expected at the site rather than taken from a single case. With a frame of 2 % damping, Λ can reach 2.8, and the slip threshold of Eq. (17) rises accordingly: for a_g = 0.45 g the critical friction

coefficient becomes 1.26 rather than 0.69. Raising the frame frequency so that $f_n T_p \geq 3.6$ keeps Λ below 1.3; for a 0.6 s pulse this means $f_n \geq 6$ Hz. This is a stiffness requirement of the same kind as the 3.5 Hz limit used against crowd excitation, but tied to the duration of the floor motion.

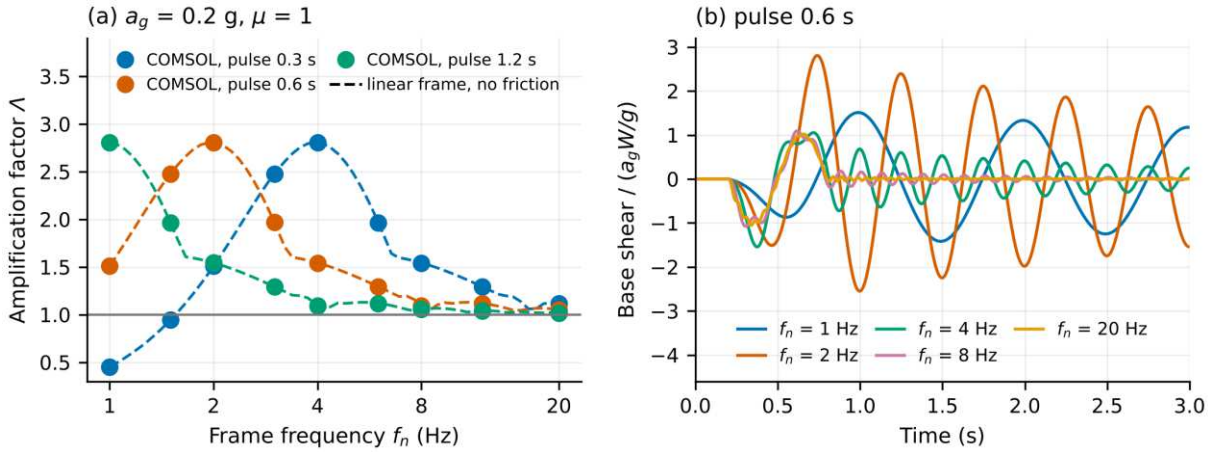


Figure 10. Amplification of the base shear by the frame (family 7, a_g = 0.2 g, μ = 1, no slip): (a) amplification factor against frame frequency for three pulse durations; the dashed lines are the linear frame without friction; (b) base shear histories for a 0.6 s pulse.

5.3 Crowd force: frequency sweep and resonance

Family 3 applies a harmonic horizontal force with an amplitude of 4 % of the weight (196 N) at μ = 0.5, which corresponds to a static index of 12.5, far above the target of 1.5. Figure 11a shows that both the frame drift and the friction force peak at resonance. The friction force cannot exceed μW = 0.5 W; in the language of structural dynamics, the interface acts as a fuse. The price is paid in slip: the slip path in 30 s is 128 mm at f/f_n = 1.0, drops to 2.4 mm at 0.95 and 1.05, and stays below about 1 mm elsewhere (Figure 11b), a band of only about ±5 % because the quality factor is 25.

Family 4 isolates the resonant case. Slip starts when the stuck frame would require a base shear above the friction capacity, which gives

$$\mu_c = Q\, F_0 / W \tag{18}$$

so that μ_c = 0.5 for F_0/W = 0.02 and 1.0 for F_0/W = 0.04 (dotted lines in Figure 11c). The simulated slip path exceeds 10 mm for $\mu \leq 0.4$ and $\mu \leq 0.8$ respectively, and decreases roughly linearly with μ below the threshold, from 246 mm at μ = 0.1 to 5.4 mm at μ = 1.0 for the larger force. The hysteresis loops (Figure 11d) are nearly rectangular, with a half-width of 0.39 mm at μ = 0.3 and 0.22 mm at μ = 0.6; the energy dissipated by friction per cycle is four times the product of friction force and half-width.

In one case (resonance, F_0/W = 0.04, μ = 1.0) the peak friction force reaches 0.99 W, which exceeds μ*W = 0.83 W for this geometry. The overturning ratio $R_{ot} = f_{max} h_{cg}/(Wb/2)$ is 1.19, so the booth would begin to rock and the pure-sliding model no longer applies. This is the situation of Figure 3b, reached here through dynamic amplification.

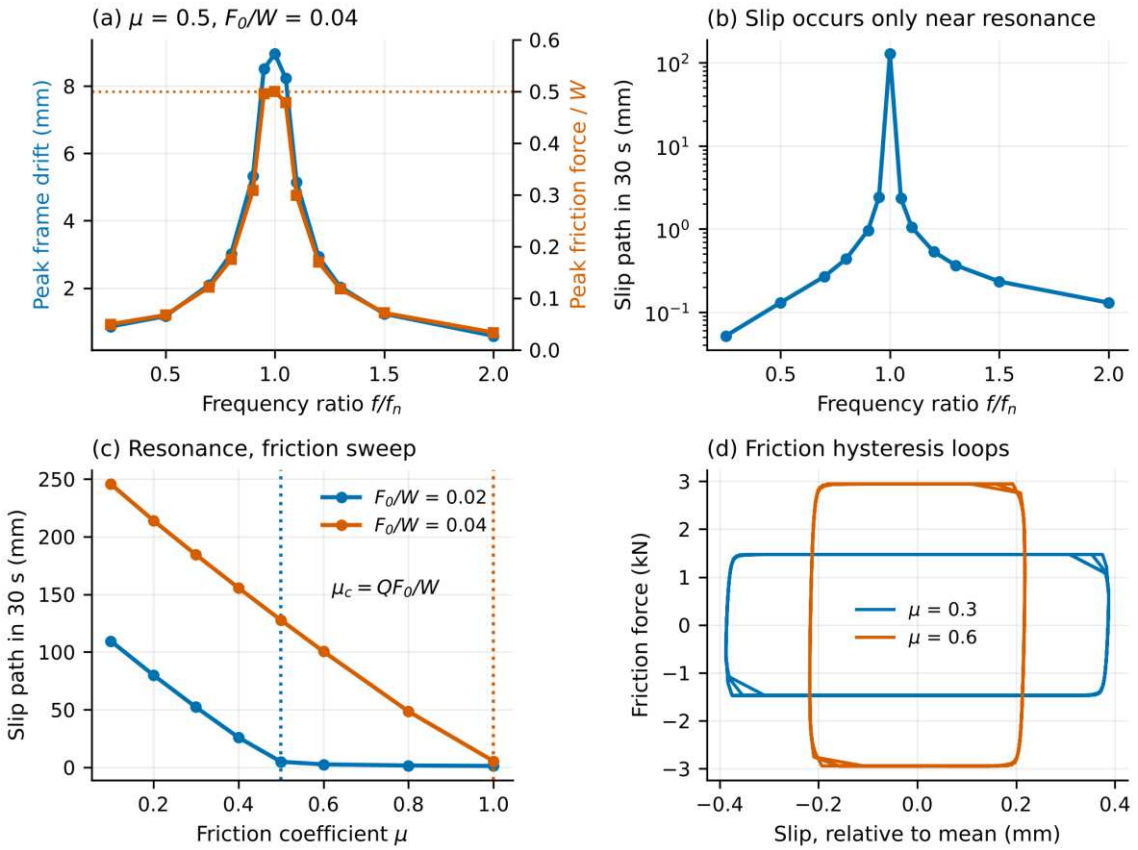


Figure 11. Crowd force: (a) peak frame drift and peak friction force against f/f_n ($\mu = 0.5$); (b) slip path in 30 s; (c) slip path against friction coefficient at resonance, with the thresholds $\mu_c = QF_0/W$ (dotted); (d) friction hysteresis loops at resonance, drawn from the stored output points of the last second of each run.

5.4 Damping and resonant slip

Eq. (18) shows that the critical friction coefficient at resonance is proportional to the quality factor $Q = 1/2\zeta$, so the damping of the frame matters as much as the friction of the interface. Family 8 repeats the resonance test with $F_0/W = 0.04$ for damping ratios of 1 %, 5 % and 10 % and friction coefficients of 0.1 to 0.6 (20 s of loading). The predicted critical coefficients are 2.0, 0.4 and 0.2 respectively (the value of 1.0 for $\zeta = 2$ % comes from Section 5.3).

Figure 12a confirms the prediction. For $\zeta = 5$ % the slip path in 20 s is 134, 86 and 42 mm at $\mu = 0.1$, 0.2 and 0.3, and only 4.3 mm at 0.4 and 1.2 mm at 0.6; for $\zeta = 10$ % it is 87 mm at 0.1, 5.7 mm at 0.2 and 0.6 to 1.3 mm above that. At μ above the critical value the friction force equals the stuck base shear QF_0 (0.40 W and 0.20 W, as predicted), and the residual slip path of 0.6 to 4 mm is micro-slip. For $\zeta = 1$ % the critical coefficient of 2.0 is out of reach, and the booth slips by 117 to 173 mm at every friction coefficient tested; the slip remains bounded, because the friction force limits the force that reaches the frame ($f/W = \mu$), but a lightly damped frame at resonance cannot be held by friction alone. At $\mu = 0.2$ the slip path in 20 s is 160 mm for $\zeta = 1$ %, 86 mm for 5 % and 5.7 mm for 10 % (Figure 12b). In terms of the threshold, raising the damping ratio from 2 % to 10 % has the same effect on resonant slip as lowering the critical friction coefficient from 1.0 to 0.2, so rubber pads and infill panels that add damping are as valuable as high-friction interfaces.

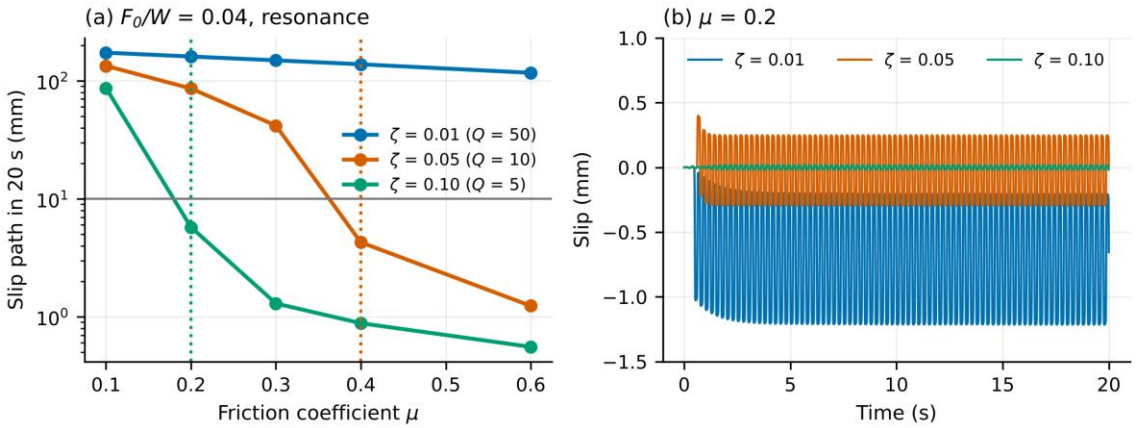


Figure 12. Damping and resonant slip (family 8, F_0/W = 0.04, resonance): (a) slip path in 20 s against friction coefficient for three damping ratios, with the predicted thresholds $\mu_c = QF_0/W$ (dotted; the value of 2.0 for ζ = 1 % lies outside the plot); (b) slip histories at μ = 0.2.

5.5 Static versus kinetic friction

Family 6 repeats a strong pulse (0.7 g) with a kinetic coefficient between 100 % and 50 % of the static one (r_k in Eq. (10)). After breakaway the base is decelerated by the lower kinetic friction, so the peak slip grows from 89 to 188 mm (×2.1) for μ_s = 0.4 and from 38 to 126 mm (×3.4) for μ_s = 0.6 (Figure 13). A design based on μ_s alone is therefore not conservative once slip has begun, and the ratio r_k should be measured alongside μ_s for each interface.

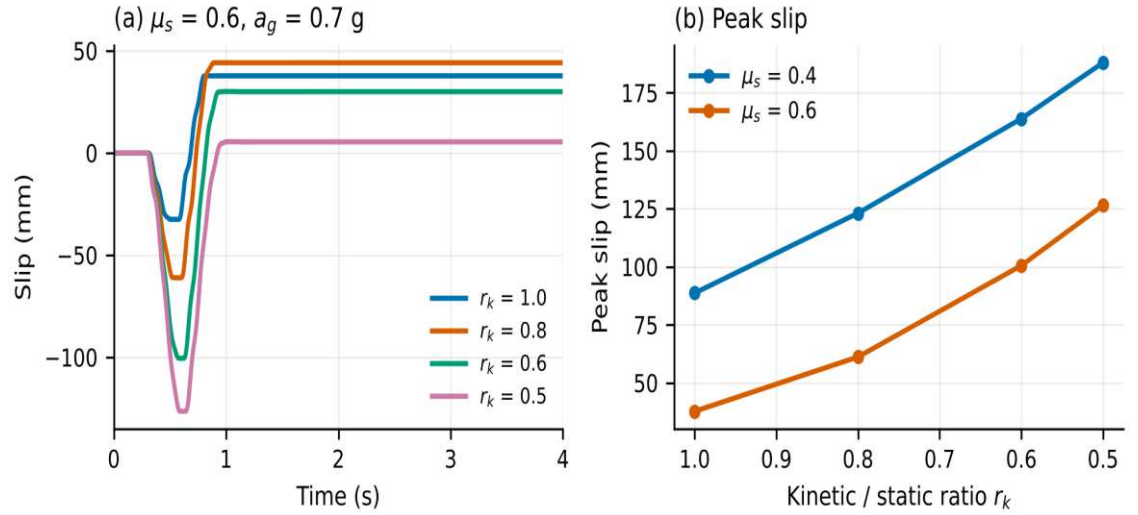


Figure 13. Static versus kinetic friction: (a) slip histories at μ_s = 0.6 for four values of r_k under a 0.7 g pulse; (b) peak slip against r_k.

5.6 Creep under vertical floor vibration

The "walking" of booths across floors does not require a force that oscillates sideways. A constant lateral load below the sliding limit is enough if the normal force dips periodically, because friction then fails for part of each cycle and the base advances in one direction only. Family 5 applies a mean lateral load of 25 % of the weight, reached smoothly in 3 s, and a vertical floor acceleration of amplitude a_{v0} at 3 Hz. Defining a dynamic index with the minimum normal force of Eq. (12),

$$\mathrm{FSI}_{\mathrm{dyn}} = \mu(1 - a_v/g) / \varphi_m, \quad \varphi_m = F_m/W \tag{19}$$

slip should begin when $FSI_{dyn} = 1$, that is, at $a_v/g = 1 - \varphi_m/\mu$. The simulations confirm this for all three friction coefficients (Figure 14). For $\mu = 0.3$ (static index 1.2) the slip after 30 s rises from 0.5 mm at 0.1 g to 154 mm at 0.2 g, with the onset predicted at 0.167 g; for $\mu = 0.4$ (index 1.6) from 0.6 mm at 0.3 g to 135 mm at 0.4 g, predicted at 0.375 g; and for $\mu = 0.5$ (index 2.0) from 0.2 mm at 0.3 g to 3.9 mm at 0.5 g and 752 mm at 0.6 g, predicted at 0.50 g. All 21 cases collapse onto the single threshold $FSI_{dyn} = 1$ (Figure 14c). Above it the creep rate is zero to within micro-slip of micrometres per cycle; below it the base moves at 5 to 32 mm/s.

This result ties the thresholds of the static framework to a physical cause. A static index of 1.5 tolerates vertical floor accelerations up to $1 - 1/1.5 = 0.33$ g before the dynamic index reaches unity, and an index of 1.2 only 0.17 g. The vertical acceleration of the supporting floor is thus a site parameter that the venue should declare; acceptance limits for floors under rhythmic crowd activity are already expressed as fractions of g [16], [40].

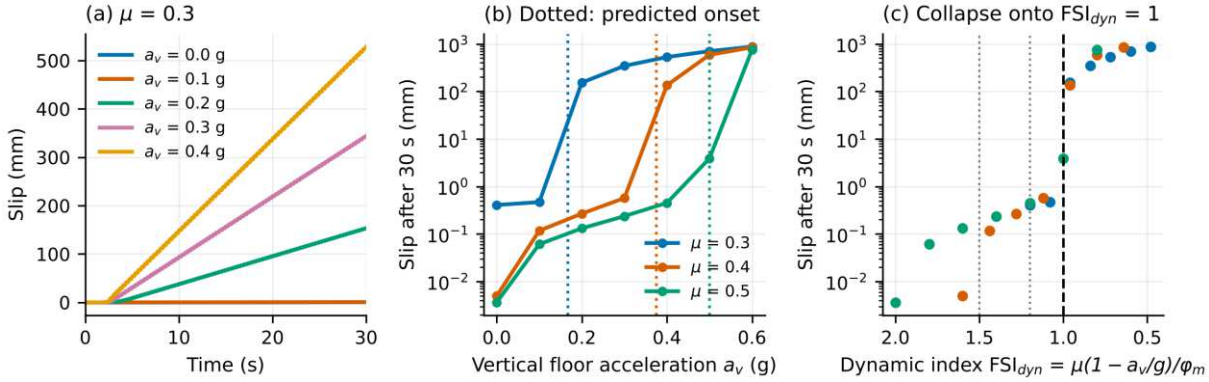


Figure 14. Creep: (a) slip histories at $\mu = 0.3$ for vertical floor accelerations of 0 to 0.4 g; (b) slip after 30 s against vertical acceleration, with the predicted onset $1 - \varphi_m/\mu$ (dotted); (c) the same data against FSI_{dyn}. Values below 1 mm are micro-slip.

The onset condition of Eq. (19) contains no reference to the frequency of the vertical vibration, but the rate of creep above the threshold does depend on it. Family 9 applies the same mean lateral load ($F_m/W = 0.25$), friction coefficient ($\mu = 0.3$) and vertical acceleration ($a_{v0} = 0.25$ g, giving $FSI_{dyn} = 0.90$) at five vibration frequencies from 1 to 8 Hz with the 4 Hz frame of the reference booth, and at three frequencies with a rigid frame ($f_n = 40$ Hz), so that the effect of the vibration can be separated from that of the frame.

All cases creep, as the criterion requires. With the rigid frame the mean creep rate over 20 s, which includes the 3 s ramp and the time to first slip, falls steadily with frequency, from 4.6 mm/s at 2 Hz to 3.5 mm/s at 3 Hz and 1.8 mm/s at 8 Hz (Figure 15b), roughly in inverse proportion to the frequency: each dip in the normal force lasts a shorter time, so the base gains less velocity during each one. With the flexible frame the rate is not monotonic: 8.5, 1.5, 8.0, 5.0 and 28.8 mm/s at 1, 2, 3, 5 and 8 Hz. The frame reduces the creep at 2 Hz (by a factor of 3 relative to the rigid frame) and increases it by a factor of 2.3 at 3 Hz and of 16 at 8 Hz, the frequency at which the vertical vibration is twice the natural frequency of the frame. The frame therefore alters the creep rate by more than an order of magnitude, in either direction, depending on the frequency ratio. The model quantifies this interaction but does not yield a simple rule for it; that would require a parametric study of the frequency ratio and damping and, above all, tests.

For design, the message is that the onset criterion remains valid and independent of frequency, while the creep rates of Section 5.6 (5 to 32 mm/s at 3 Hz) apply only to the booth and frequency tested. A booth whose frame frequency lies close to a harmonic of the floor vibration frequency, as under rhythmic activity, should be assumed to creep faster than the rigid-body estimate.

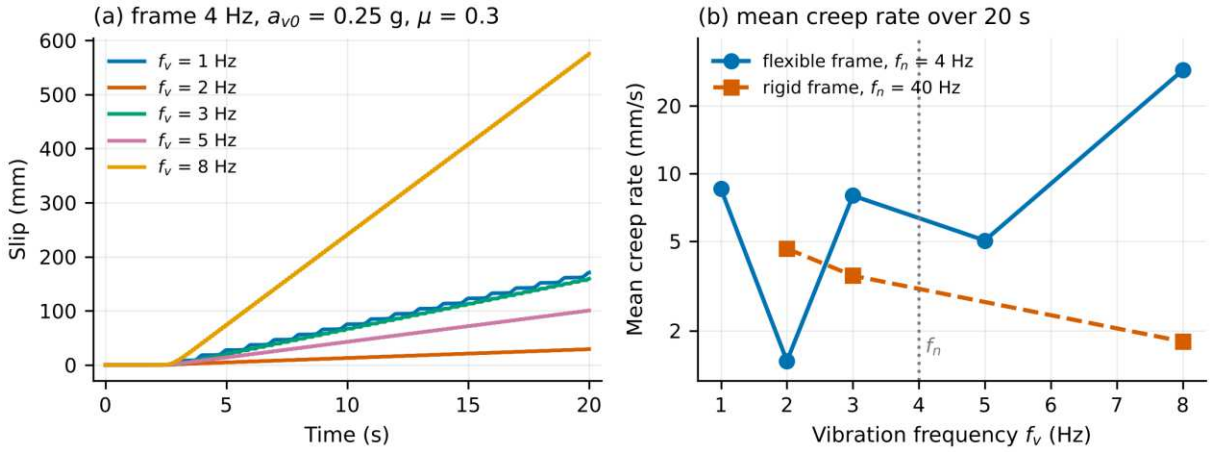


Figure 15. Creep and the frequency of the vertical vibration (family 9, μ = 0.3, a_{v0} = 0.25 g, F_m/W = 0.25): (a) slip histories for the flexible frame at five frequencies; (b) mean creep rate over 20 s for the flexible frame (f_n = 4 Hz) and for a rigid frame (f_n = 40 Hz).

5.7 Probability of sliding under vertical vibration

The probabilistic argument of Eq. (7) carries over directly. Replacing the critical coefficient $\mu_c = F_h/N$ with one that includes the minimum normal force,

$$\mu_c = \varphi / (1 - a_v/g) \tag{20}$$

in Eq. (7) gives, for $\bar{\mu}$ = 0.5 and σ = 0.10, a sliding probability at a design index of 1.5 of 4.8 % without vertical vibration, 9.7 % at 0.1 g, 20.2 % at 0.2 g and 40.6 % at 0.3 g (Figure 16a). The 20 % that Section 3.4 attributes to an index of 1.2 is therefore reached at an index of 1.5 under a vertical floor acceleration of 0.2 g. Holding the 4.8 % level under a vertical acceleration a_v requires a static index of $1.5/(1 - a_v/g)$: 1.67 at 0.1 g, 1.88 at 0.2 g and 2.14 at 0.3 g.

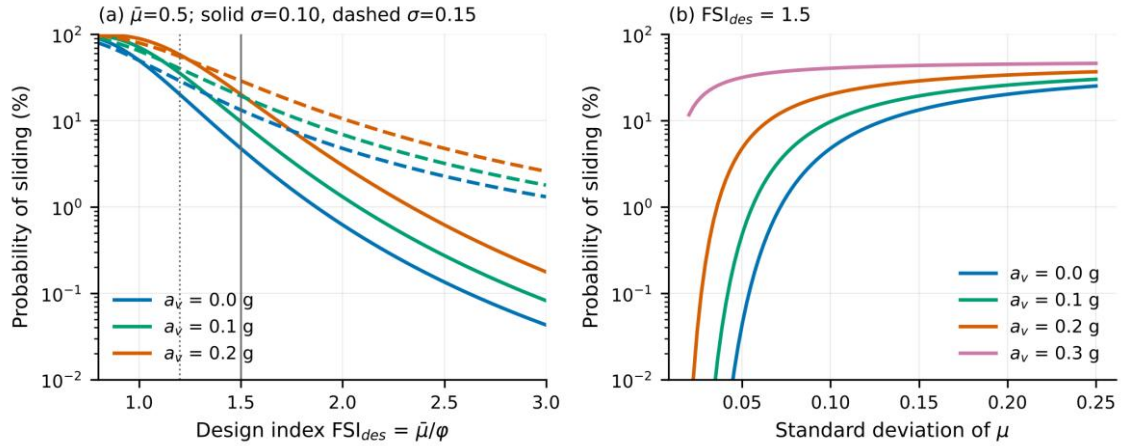


Figure 16. Probability of sliding for a normally distributed friction coefficient ($\bar{\mu}$ = 0.5): (a) against the design index for σ = 0.10 (solid) and 0.15 (dashed) and vertical floor accelerations of 0, 0.1 and 0.2 g; (b) against σ at a design index of 1.5.

5.8 Summary of the thresholds

Table 8 compares the thresholds predicted by the closed-form expressions with those found in the simulations. In every case examined, the simulated onset lies within the bracket that contains the prediction.

Table 8. Slip thresholds: closed-form prediction against simulation (slip criterion: peak slip ≥ 1 mm for pulses and creep, slip path ≥ 10 mm for resonance).

Family	Governing relation	Case	Predicted onset	Simulated onset between
2	$\mu_c = \Lambda a_g/g$, $\Lambda = 1.54$	$a_g = 0.20$ g	$\mu = 0.31$	0.2 and 0.3
2		$a_g = 0.30$ g	$\mu = 0.46$	0.4 and 0.5
2		$a_g = 0.45$ g	$\mu = 0.69$	0.6 and 0.7
4	$\mu_c = QF_0/W$, $Q = 25$	$F_0/W = 0.02$	$\mu = 0.50$	0.4 and 0.5
4		$F_0/W = 0.04$	$\mu = 1.00$	0.8 and 1.0
5	$a_v/g = 1 - \varphi_m/\mu$, $\varphi_m = 0.25$	$\mu = 0.3$	0.167 g	0.1 and 0.2 g
5		$\mu = 0.4$	0.375 g	0.3 and 0.4 g
5		$\mu = 0.5$	0.500 g	0.4 and 0.5 g
8	$\mu_c = QF_0/W$, $F_0/W = 0.04$	$\zeta = 0.10$ ($Q = 5$)	$\mu = 0.20$	0.1 and 0.2
8		$\zeta = 0.05$ ($Q = 10$)	$\mu = 0.40$	0.3 and 0.4
8		$\zeta = 0.01$ ($Q = 50$)	$\mu = 2.00$	above 0.6 (slip at all values)

6. Case Studies and Design Application

6.1 Exhibition booths

The framework was applied to three modular exhibition booths that had been modelled in SAP2000. The support reactions were taken from the analysis under the governing service load combination (wind and crowd loads), and the index was evaluated at the most heavily loaded support with the steel-on-concrete coefficient $\mu = 0.5$, which falls within the 0.3–0.6 range of Figure 2.

The Vision Booth (Figure 17) is a single-deck steel frame of SHS 100 members with 300 mm × 300 mm base plates. Figure 18 shows the reactions of the SAP2000 model. At the most loaded support the vertical reaction is V = 33.44 kN, and the horizontal components of 1.44 kN and 1.03 kN combine to a resultant of H = 1.76 kN (1.77 kN from the rounded components). The friction capacity is $\mu V = 16.7$ kN and $FSI_s = 9.50$. The SBA Booth (Figure 19) is a double-deck system of IPE 180 and HEB 200 profiles with 500 mm × 500 mm × 20 mm base plates; with V = 86.7 kN and H = 4.1 kN the friction capacity is 43.4 kN and $FSI_s = 10.57$. The IMH Booth is a two-storey modular structure with internal stairs, glass infill and 600 mm × 600 mm × 20 mm base plates; with V = 75.8 kN and H = 2.0 kN, $FSI_s = 18.95$. Table 9 and Figure 20 summarise the results.

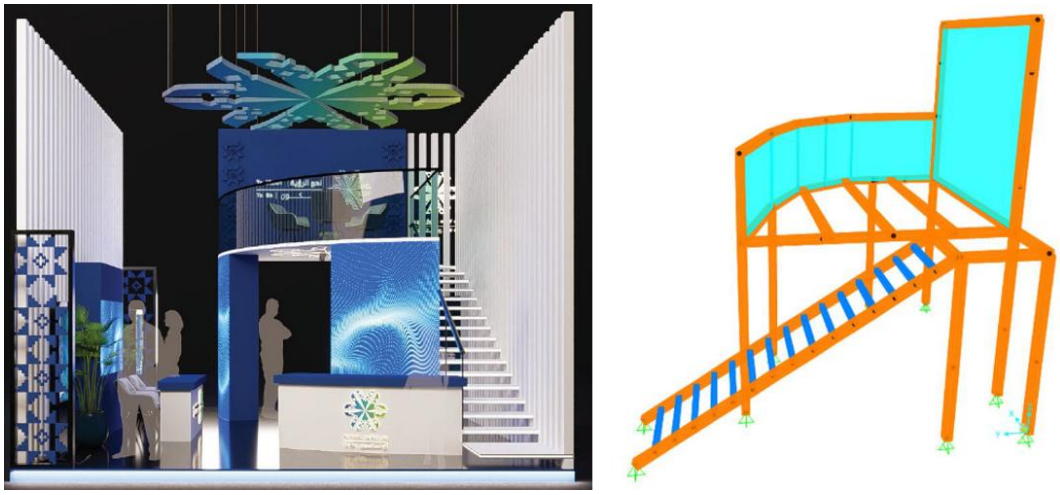


Figure 17. Vision Booth: (left) architectural view; (right) SAP2000 numerical model.

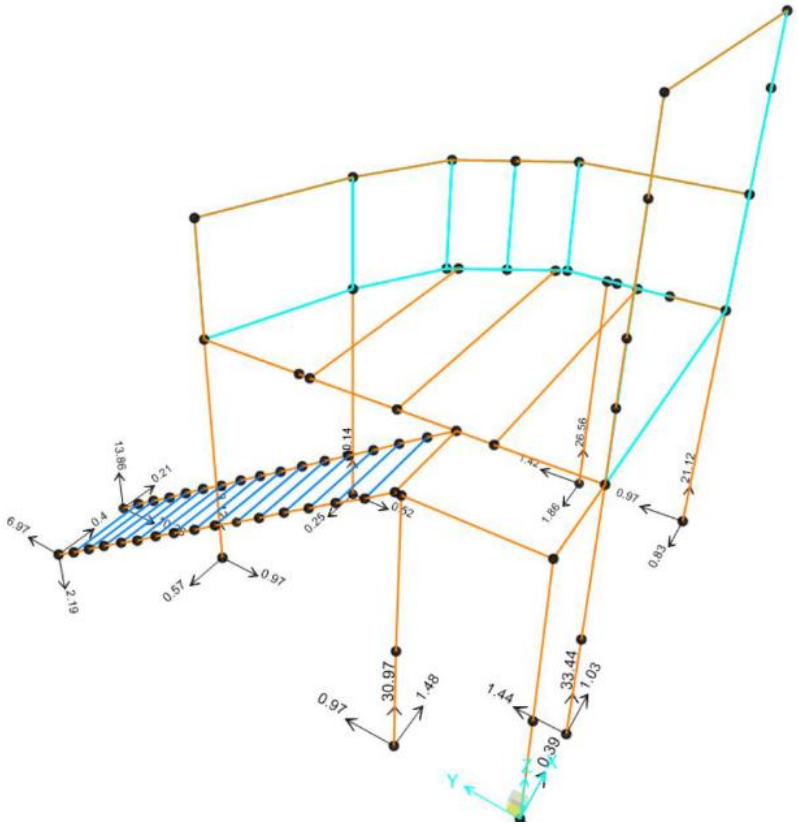


Figure 18. Vertical and horizontal support reactions (kN) from SAP2000 for the Vision Booth, used to compute the frictional resistance.

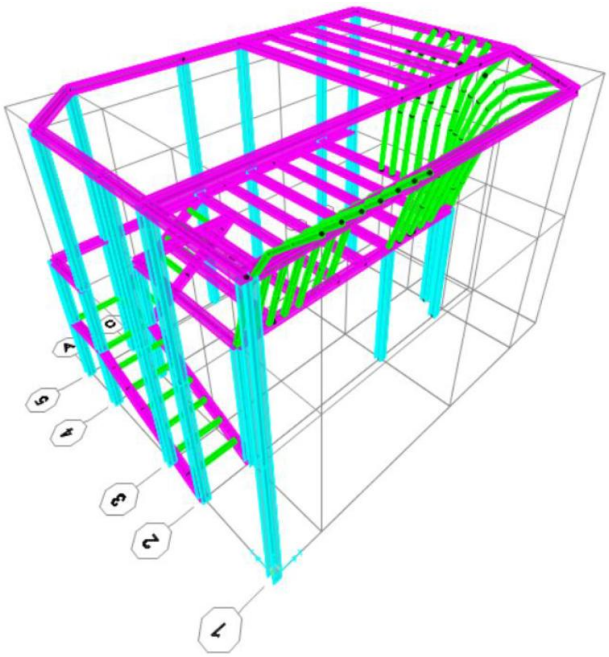


Figure 19. Numerical model of the SBA Booth.

Table 9. Static stability of the three booths at the most heavily loaded support (μ = 0.5, service load combination).

Booth	Configuration	Base plate	Plate area (m²)	V (kN)	H (kN)	FSI_s	Class
Vision	Single deck	300 × 300 mm	0.09	33.44	1.76	9.50	Stable
SBA	Double deck	500 × 500 × 20 mm	0.25	86.7	4.10	10.57	Stable
IMH	Double deck	600 × 600 × 20 mm	0.36	75.8	2.00	18.95	Stable

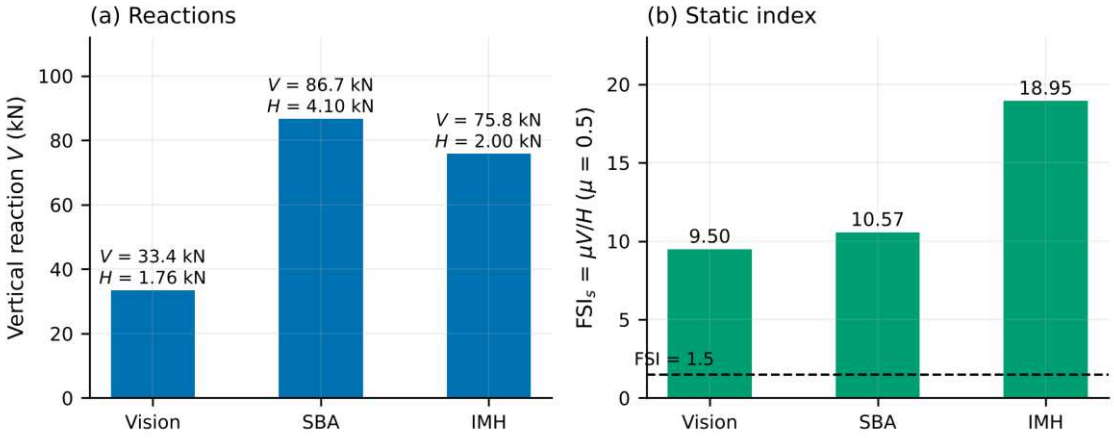


Figure 20. (a) Vertical reaction and horizontal resultant at the critical support of the three booths; (b) static index FSI_s for μ = 0.5 against the target of 1.5.

All three booths exceed the target of 1.5 by a wide margin under service loads, and the ranking is governed by the ratio V/H rather than by weight alone: the IMH Booth is lighter than the SBA Booth yet has the larger index because its horizontal demand is much smaller. A 20 % reduction

in μ (through dust, for instance) lowers the index in proportion, which would matter only for marginal designs. Two limits of this evaluation should be kept in mind. The reactions derive from service loads, not floor motion, so the margin does not cover an earthquake or a vibrating floor; for the reference frame and a 0.6 s pulse, Eq. (17) predicts that a coefficient of 0.5 is exceeded once the floor acceleration passes about 0.5/1.54 = 0.32 g, and Eq. (19) shows how the vertical floor acceleration erodes the margin, both limits depending on the dimensionless parameters rather than on the mass of the booth. The second limit is that the index is evaluated per support; the global check uses the sum of the reactions, and the two should be compared in a design.

To illustrate the role of the interface, consider a booth with an elevated centre of gravity standing on high-gloss polished marble with μ = 0.25 under a demand φ = 0.32, which gives FSI_s = 0.78. Replacing the bare base with a rubber sub-base of μ = 0.8 would raise the index to 2.5 without any change to the frame, provided the tipping limit μ* is checked. The example is hypothetical, but it makes the point that failures of non-anchored booths tend to originate in the interface rather than in the structure.

6.2 Seismic example

The seismic example follows ASCE 7-22. A standard booth of 500 kg (W_p = 4.905 kN) stands on a ground-level slab (z/h = 0) in a high-seismic region (S_{DS} = 1.0 g) with I_p = 1.5. Two interfaces are considered: metal on polished marble (μ = 0.3, scenario A) and a rubber-coated base (μ = 0.7, scenario B). With the 2016-edition equation, which uses a_p = 1.0 and R_p = 2.5, the lateral demand is F_p = 1.18 kN, and the static indices are 1.25 for scenario A, below the target of 1.5, and 2.92 for scenario B.

The lower bound of Eq. (6), however, is $F_{p,min} = 0.3\ S_{DS}\ I_p\ W_p$ = 2.21 kN, which exceeds 1.18 kN, so the lower bound governs. Table 10 shows the consequences. The low-friction case becomes unstable (0.67 instead of 1.25), and the rubber case only just reaches the target (1.56 instead of 2.92). The lower-bound force corresponds to a floor acceleration of 0.45 g for this booth, and with the amplification of Section 5.1 the dynamic index of the rubber case is 1.01. This agrees with the simulation, in which the peak slip stays below 0.03 mm: no slip, but no margin either. The low-friction case slips by 42 mm in the simulation. Where the response of the booth is dominated by the frame (C_{AR} > 1), the demand and the amplification must be assessed together. The amplification of 1.54 belongs to a 4 Hz frame and a 0.6 s pulse; for a 0.3 s pulse the same frame has $f_n T_p$ = 1.2 and Λ = 2.81 (Section 5.2), and the dynamic index of the rubber case falls to 0.55, so the interface that just passes in Table 10 would slip. The pulse duration and the frame frequency must therefore be stated together with the design acceleration.

Table 10. Seismic example recomputed with the lower-bound design force (W_p = 4.905 kN, S_{DS} = 1.0 g, I_p = 1.5).

Interface	μ	FSI_s with F_p = 1.18 kN	FSI_s with $F_{p,min}$ = 2.21 kN	$FSI_{dyn,p}$ (Λ = 1.54)	Simulated peak slip, 0.45 g pulse
Metal on polished marble	0.3	1.25	0.67	0.43	42 mm
Rubber-coated base	0.7	2.92	1.56	1.01	0.03 mm

7. Design Framework

7.1 A family of indices

The results argue for retaining the capacity–demand format of the FSI and the target of 1.5, but evaluating it against the demand that actually governs. Table 11 collects the indices; each has a verified onset of slip at the value 1.0 (Sections 4.4 and 5).

Table 11. Proposed family of stability indices (target value 1.5 for each applicable index; slip onset verified at 1.0).

Index	Definition	Governing situation
FSI_s	$\mu N/F_h$	slow or quasi-static horizontal load, Eq. (1)
FSI_{eff}	$\min(\mu, b/2h_{cg}) / \varphi$	tall or narrow booths; high-friction interfaces, Eq. (3)
$FSI_{dyn,p}$	$\mu g / (\Lambda a_g)$	floor pulse or earthquake, flexible frame, amplification Λ, Eq. (17)
$FSI_{dyn,r}$	$\mu W / (Q F_0)$	harmonic crowd force near the frame frequency, Eq. (18)
$FSI_{dyn,v}$	$\mu(1 - a_v/g) / \varphi_m$	mean lateral load with vertical floor vibration, Eq. (19)

Where an index falls below target, ballast raises FSI_s, $FSI_{dyn,r}$ and $FSI_{dyn,v}$ in proportion only if the demand does not grow with the mass; a rubber pad raises all of them but must be checked against μ^* (Eq. (4)). The amplification factor Λ depends on the product of frame frequency and pulse duration and tends toward 1 as the frame frequency is raised well above the frequency content of the floor motion (Section 5.2), while the quality factor Q falls as damping is increased (Section 5.4). Frame stiffness and damping are therefore design variables of the same standing as the interface.

7.2 Implementation workflow

A four-step workflow translates the indices into on-site practice (Figure 21).

Step 1: Surface classification. Before installation the venue floor is classified by finish and expected friction coefficient. Common surfaces in Saudi exhibition environments include polished marble, epoxy-coated slabs and power-troweled concrete. If the estimated coefficient is $\mu \leq 0.30$, the design must include an interface enhancement. The static and kinetic coefficients should be measured on site where possible, together with the vertical acceleration of the floor.

Step 2: Load and occupancy assessment. Peak crowd loading, particularly near stages and access points, is evaluated in accordance with the applicable code for assembly occupancies, and the seismic demand follows Section 3.3 including its lower bound. Where high lateral demand is expected, the interface is upgraded so that every applicable index stays at or above 1.5.

Step 3: Interface modification. Bare aluminium or plywood bases are replaced with vulcanised rubber pads (60–70 Shore A) or equivalent high-friction gaskets, and the tipping limit μ^* is checked. Increased friction also lowers the resonant response of Section 5.3 and the creep of Section 5.6.

Step 4: Stability certification. For approval by the authority having jurisdiction, a stability statement is issued: "The stand structure achieves an index of [value] for each applicable demand in Table 11, exceeding the target of 1.5, in accordance with the project design criteria; reliance on friction is submitted as a performance-based alternative to anchorage." The statement is a proposal of this study and not an existing code requirement.

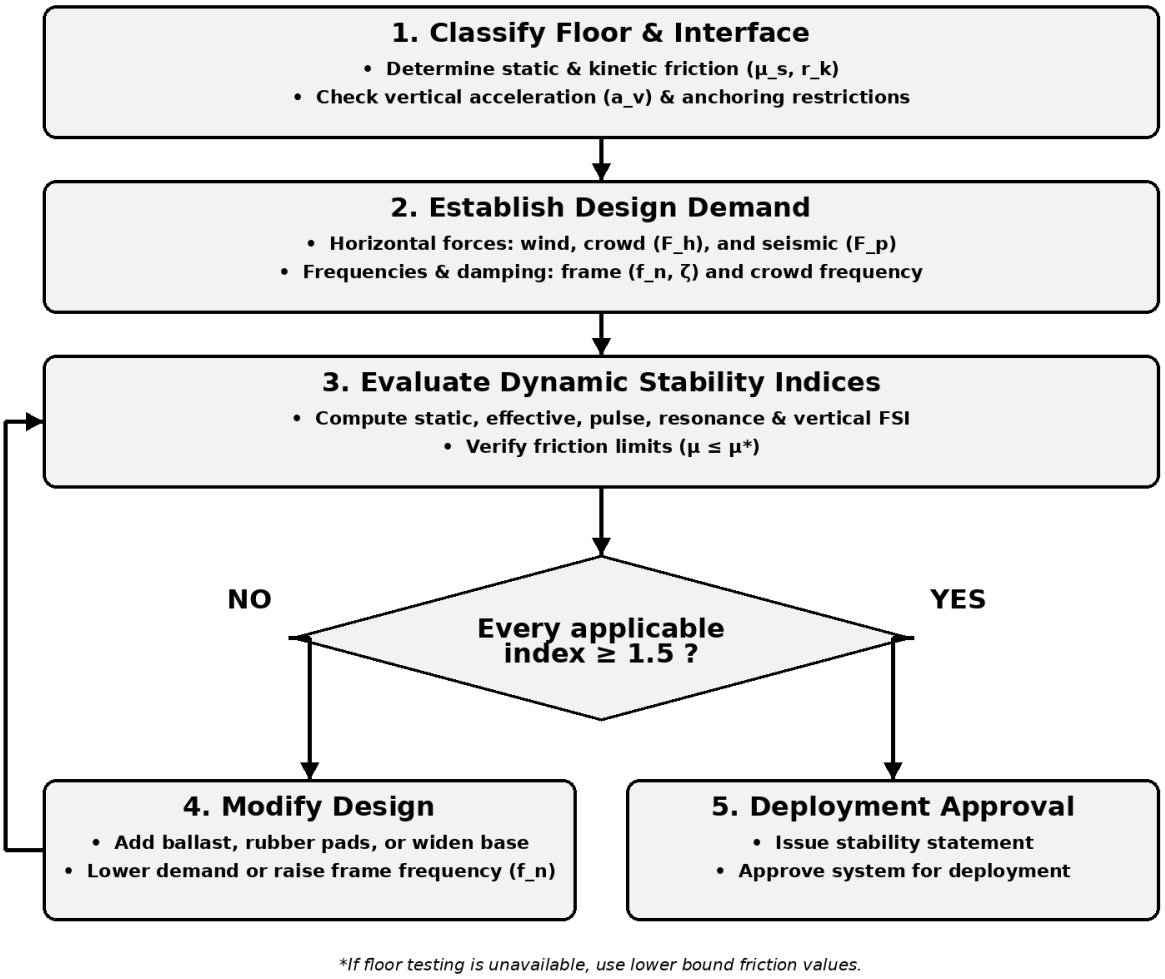


Figure 21. On-site deployment and compliance workflow for non-anchored booths.

8. Sustainability, Circularity and Land-Use Implications

8.1 Environmental implications of the stabilization method

Mechanical anchoring requires drilling into finished floors, which causes local damage, demands epoxy grout and post-event remediation, and leaves single-use anchor hardware that cannot be reused. Friction-based stabilization relies instead on interfacial shear resistance, provided for example by rubber pads or textured base plates; it preserves the integrity of the venue substrate and allows all base components to be reused. Table 12 compares the two methods qualitatively and Figure 22 illustrates the difference. The comparison is deliberately qualitative: a life-cycle assessment with defined system boundaries is needed before the saving in material and carbon can be quantified.

Table 12. Environmental and operational implications of mechanical anchoring and friction-based stabilization (qualitative).

Stabilization method	Floor damage	Reusability	Anchor waste	Expected carbon impact
Mechanical anchors	Yes	Low	High	Higher
Friction-based	No	High	None	Lower

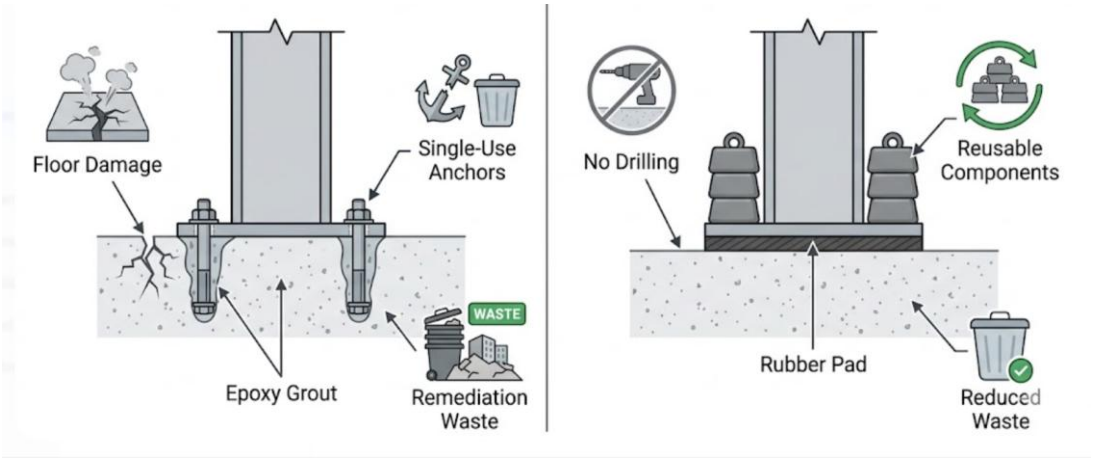


Figure 22. Mechanical anchoring (left) and friction-based stabilization (right): conceptual illustration.

8.2 Circularity

Frameworks of key performance indicators for circular buildings span material, waste, energy, water, emissions and design, and rank disassembly, avoidance of unnecessary new construction and material durability highest [41], [42]. Reuse carries the greatest weight in the material and waste categories, which supports a stabilization method that consumes no components. These strategies align with the circular-economy frameworks developed for the built environment [43], [44]. Reducing embodied emissions calls for material optimisation together with a systemic change in practice, including modularity, demountability and reversible assembly [45]. Embodied-carbon studies of modular construction report reductions through shorter construction time, less waste and optimised material use [46], [47], and city-scale analyses show that modular supply chains redistribute embodied carbon between production, transport and reuse [48]; design for disassembly is associated with higher rates of resource recovery [49]. A reusable shoring system is reported to save more than 50 % of the emissions of conventional temporary works [50]. Indicator-based circular-city frameworks connect such measures to Sustainable Development Goal 11 [51]. None of these studies addresses friction-based stabilization itself, so the benefit of removing anchors and floor repair is argued here qualitatively, and its magnitude remains to be quantified.

8.3 Land use and urban planning

Temporary use has become a planning tool for activating underused spaces, testing urban regeneration strategies and supporting flexible land-use transitions without permanent change [52]–[56]. Pop-up and modular structures conceived as temporary from the outset, with lightweight technologies, rapid assembly and occupation of the ground without alteration, are consistent with a friction-based approach [57]. Because a friction-stabilized structure leaves the site as it found it, it supports reversible occupation of plazas, exhibition halls, transit nodes and

heritage-sensitive settings where invasive anchoring is unacceptable. The ability to deploy without ground works also helps in crisis situations such as disaster response or extreme heat. At the municipal scale the framework supports event-infrastructure planning and time-bound programming that preserves landscape assets, in line with definitions of urban resilience that emphasise adaptability and recoverability [29].

8.4 Applications beyond exhibitions

The same index applies to other temporary structures on smooth floors. Pop-up retail kiosks and mobile shops in malls, plazas and transit hubs rely on lightweight freestanding frames that must resist accidental impacts and crowd surges. Emergency shelters and field hospitals are deployed on terrain ranging from polished concrete to packed soil, where anchoring may be impossible. Mobile work platforms and modular scaffolding on smooth industrial floors are prone to walking under worker movement or machinery, which the creep threshold of Section 5.6 addresses directly. Outdoor stages face crowd-induced vibration and wind, and combinations of rubberised mats and ballast can provide a safety factor without permanent footings. In each case the governing index of Table 11 depends on the situation, and the interface and the floor must be characterised before the index is trusted.

9. Limitations and Future Work

The dynamic model describes one horizontal direction and a lumped frame; two-way motion, torsion and the interaction of several stands are not covered. Rocking is checked through the overturning ratio and the criterion of Eq. (4) but is not simulated. The pre-slip length, the Stribeck velocity and the damping ratio are assumed values, and the frequency, amplitude and shape of the excitations are parameters rather than measurements. The friction coefficients are deterministic inputs whose scatter enters only through Eqs. (7) and (20). The results are therefore a numerical verification of the stability indices and of their failure thresholds, and they should be calibrated with tilting-table or pull tests of the real interface and with measured frame properties before being used as design values. The case studies use service-load reactions and a single friction coefficient and do not include earthquake or floor-vibration demands. The peak values stored by the COMSOL monitors lag by a few milliseconds, which matters only for the stiffest frames under sharp pulses, and one case (65) shows a numerical drift of 0.4 mm that was not repeated with a tighter tolerance (Section 4.4). Finally, ASCE 7 requires positive attachment, so any use of the framework as a substitute for anchorage requires the acceptance of the authority having jurisdiction.

Future work should include (i) laboratory and field measurements of static and kinetic friction on real venue floors, including the effect of contamination and wear, possibly through a degradation modifier on μ; (ii) shake-table and pull tests of freestanding booths to calibrate the pre-slip, Stribeck and damping parameters; (iii) a two-way model with rocking; (iv) a life-cycle assessment of friction-based and anchored stabilization with defined system boundaries; and (v) smart or textured interface materials and monitoring systems that measure slip in service.

10. Conclusions

This study proposes a friction-based stabilization framework for non-anchored temporary installations and tests it with a verified dynamic model and 143 parametric cases. The conclusions are as follows.

- The static index $FSI = \mu N/F_h$ is the exact threshold for slow sliding, but the combined index $FSI_{eff} = \min(\mu, b/2h_{cg})/\varphi$ should be used, because raising μ beyond $b/2h_{cg}$ shifts the failure from sliding to overturning.
- A flexible frame amplified the base shear by a factor of 1.54 under a 0.6 s floor pulse, so slip began at $\mu_c = 1.54\, a_g/g$ rather than a_g/g. The amplification depends only on the product of frame frequency and pulse duration, reaching 2.8 at $f_nT_p = 1.2$ and staying below 1.3 for $f_nT_p \geq 3.6$, so a stiff frame is a remedy as effective as a high friction coefficient.
- At resonance the friction force limits the force transmitted to the frame to μW, at the cost of slip within a band of about ±5 % around the natural frequency, and slip starts at $\mu_c = QF_0/W$. Because the threshold is proportional to the quality factor, a damping ratio of 10 % lowers the critical coefficient from 1.0 to 0.2 for $F_0/W = 0.04$, whereas 1 % cannot be held by friction at any realistic value (critical coefficient 2.0).
- Creep under a mean lateral load starts at $FSI_{dyn} = \mu(1 - a_v/g)/\varphi_m = 1$; a static index of 1.5 tolerates a vertical floor acceleration of 0.33 g and an index of 1.2 only 0.17 g. A kinetic coefficient of half the static one doubles the peak slip or more than triples it.
- Slip thresholds from the closed forms and from the simulations agree in all cases checked (Table 8).
- The COMSOL implementation reproduces the closed-form tests to within 1.6 % at the default pre-slip length and 0.4 % at the finest one, and its energy balance closes to better than 10^{-3} in every case.
- The lower-bound seismic force of ASCE 7-22 can govern the design: for a 500 kg booth with $S_{DS} = 1.0$ g and $I_p = 1.5$ it is 2.21 kN and reduces the index of a rubber-coated base from 2.92 to 1.56, which leaves no margin once the dynamic amplification is included.
- The three exhibition booths have static indices of 9.5 to 19 for service loads, well above the target of 1.5, but this margin does not cover floor motion.

Beyond the structural results, friction-based stabilization allows temporary structures to be deployed without damaging the host surface, supports reversible land occupation and the reuse of components, and gives planners and engineers a shared quantitative language for temporary installations. Its use as a substitute for anchorage requires acceptance by the authority having jurisdiction, because current codes require positive attachment, and the numerical thresholds require calibration by tests of the actual interface. Within these limits the framework offers a scalable pathway toward reversible, resilient and circular temporary urban infrastructure, in support of Sustainable Development Goals 9, 11 and 12.

Nomenclature

Symbol	Description	Unit
μ, μ_s	Static coefficient of friction	–
r_k	Ratio of kinetic to static friction	–

Symbol	Description	Unit
FSI, FSI_s	Frictional Stability Index (sliding)	–
FSI_o, FSI_{eff}	Overturning index; combined index	–
$FSI_{dyn,p}$, $FSI_{dyn,r}$, $FSI_{dyn,v}$	Dynamic indices (pulse, resonance, vertical vibration)	–
N, W	Normal force; weight	kN
F_h, φ	Horizontal demand; demand as a fraction of W	kN; –
b, h_{cg}	Base width; height of the centre of gravity	m
μ*	Friction coefficient at which sliding and tipping coincide, $b/2h_{cg}$	–
F_p, S_{DS}, I_p, W_p	Seismic force, design spectral acceleration, importance factor, component weight	kN, g, –, kN
H_f, R_μ, C_{AR}, R_{po}	ASCE 7-22 height, ductility, resonance and strength factors	–
m, m_b, k, c	Upper mass, base mass, frame stiffness, frame damping	kg, kg, N/m, N·s/m
f_n, ζ, Q	Natural frequency, damping ratio, quality factor 1/2ζ	Hz, –, –
s, u, z, δ	Slip; frame drift; Dahl state; pre-slip length	mm, mm, –, mm
a_g, a_v	Horizontal and vertical floor acceleration	m/s²
Λ	Amplification factor of the base shear	–
F_0, F_m, f_F	Amplitude, mean and frequency of the horizontal force	N, N, Hz
$\bar{\mu}$, σ, P_{slide}	Mean and standard deviation of μ; probability of sliding	–, –, –
ε_E	Energy residual (Eq. (16))	–
W_{in}, E_k, E_e, D_v, D_f	Work of the loads; kinetic and elastic energy; viscous and frictional dissipation	J
v, w	Slip velocity; drift velocity	mm/s
a_0, T_p	Amplitude and duration of the floor-acceleration pulse	g, s
τ_M	Relaxation time of the running-maximum monitors	s

Declarations

Competing interests. The authors declare no known competing financial interests or personal relationships that could have influenced the work reported in this paper.

Authors' contributions. MTN conceptualised the study, conducted the structural analysis and the numerical modelling, and led the writing of the manuscript. AF provided technical insights,

contributed to the comparative code analysis, reviewed the case studies and helped refine the final draft.

Funding. This research received no external funding.

Data availability statement: All data generated or analysed during this study are included in this published article.

Use of AI tools. Artificial intelligence tools (Grammarly, ChatGPT and Claude) were used to assist with language editing. The authors reviewed and verified all content and take full responsibility for it.

Ethics, Consent to Participate, and Consent to Publish declarations: NA.

References

[1] United Nations Environment Programme and Global Alliance for Buildings and Construction, *Global Status Report for Buildings and Construction: Beyond Foundations: Mainstreaming Sustainable Solutions to Cut Emissions from the Buildings Sector*. Nairobi: UNEP, 2024.

[2] Y. Li *et al.*, "Energy-related carbon emissions in the building sector: Drivers, forecasting, and multi-scenario analysis," *Energy Reports*, vol. 15, p. 109128, Jun. 2026, doi: 10.1016/J.EGYR.2026.109128.

[3] I. Shkalei *et al.*, "Effect of climatic and thermal aging on friction of frost-resistant rubber with and without ultra-high molecular weight polyethylene coating," *Coatings*, vol. 15, no. 5, 2025, doi: 10.3390/coatings15050514.

[4] D. D'Angela, A. Contento, G. Kampas, and G. Magliulo, "Seismic response of rocking-dominated nonstructural elements: a comprehensive review," *J. Earthq. Eng.*, 2025, doi: 10.1080/13632469.2025.2525911.

[5] F. Wang, Y. Huang, and Z. Qu, "Limitation of base isolation in protecting freestanding contents in buildings," *Earthq. Eng. Struct. Dyn.*, vol. 52, no. 6, 2023, doi: 10.1002/eqe.3844.

[6] M. T. Naqash, C. Bedon, and A. Formisano, "Structural design of balustrades: code compliance, cross-section requirements and case studies," *Structures*, vol. 87, p. 111763, May 2026, doi: 10.1016/J.ISTRUC.2026.111763.

[7] R. P. Dhakal, "Seismic design of buildings: where to next?," *Bull. N. Z. Soc. Earthq. Eng.*, 2024, doi: 10.5459/bnzsee.1680.

[8] D. H. Chung and J. H. Won, "Experimental study on the rotational stiffness of pocket type scaffolding connection according to the rotation direction," *Appl. Sci.*, vol. 13, no. 9, 2023, doi: 10.3390/app13095500.

[9] EN 13893:2002, *Resilient, laminate and textile floor coverings — Measurement of dynamic coefficient of friction on dry floor surfaces*. Brussels: CEN, 2002.

[10] H. L. Costa, J. Schille, and A. Rosenkranz, "Tailored surface textures to increase friction—a review," *Friction*, 2022, doi: 10.1007/s40544-021-0589-y.

[11] R. Subramani, R. R. Leon, R. Nageswaren, M. A. Rusho, and K. V. Shankar, "Tribological performance enhancement in FDM and SLA additive manufacturing: materials, mechanisms, surface engineering, and hybrid strategies — a holistic review," *Lubricants*, vol. 13, 2025, doi: 10.3390/lubricants13070298.

[12] G. Aswin *et al.*, "Recent advances in corrosion behaviour and interfacial failure of rubber–metal composites," *npj Mater. Degrad.*, vol. 10, no. 1, 2025, doi: 10.1038/s41529-025-00721-4.

[13] M. T. Naqash and A. Formisano, "A conceptual framework for pollution-resilient aluminium façades: introducing the Pollution Degradation Modifier (PDM)," *Buildings*, vol. 16, no. 4, Feb. 2026, doi: 10.3390/buildings16040861.

[14] European Commission, "Buildings and construction," Internal Market, Industry, Entrepreneurship and SMEs. [Online]. Available: https:*single-market-economy.ec.europa.eu/industry/sustainability/buildings-and-construction_en (accessed Oct. 8, 2026).*

[15] O. Kocaer, A. Kul, and A. Aldemir, "From principles to practice: a systematic literature review of design for manufacture and assembly and design for deconstruction strategies for a circular construction industry," *Struct. Concr.*, 2026, doi: 10.1002/suco.70452.

[16] H. Bachmann and W. Ammann, *Vibrations in Structures Induced by Man and Machines*, IABSE Structural Engineering Document 3e. Zürich: IABSE, 1987.

[17] S. Živanović, A. Pavic, and P. Reynolds, "Vibration serviceability of footbridges under human-induced excitation: a literature review," *J. Sound Vib.*, vol. 279, no. 1–2, pp. 1–74, 2005.

[18] A. Caloni, M. Morfino, M. Civera, and C. Surace, "Structure-to-human interaction (H2SI): pedestrian response to oscillating footbridges and considerations on their structural control and health monitoring," *Infrastructures*, vol. 10, no. 1, 2025, doi: 10.3390/infrastructures10010009.

[19] K. Van Nimmen, A. Pavic, and P. Van den Broeck, "A simplified method to account for vertical human-structure interaction," *Structures*, vol. 32, pp. 2004–2019, Aug. 2021, doi: 10.1016/J.ISTRUC.2021.03.090.

[20] C. Zhao and T. Ji, "Predicting responses of a human-structure interaction system subjected to rhythmic crowd loads," *J. Build. Eng.*, vol. 116, p. 114522, Dec. 2025, doi: 10.1016/J.JOBE.2025.114522.

[21] P. Liu, Y. M. Zhang, H. T. Chen, and W. G. Yang, "Experimental study on rocking blocks subjected to bidirectional ground and floor motions via shaking table tests," *Earthq. Eng. Struct. Dyn.*, vol. 52, no. 10, 2023, doi: 10.1002/eqe.3918.

[22] D. D'Angela, G. Magliulo, and E. Cosenza, "Incremental dynamic analysis of rigid blocks subjected to ground and floor motions and shake table protocol inputs," *Bull. N. Z. Soc. Earthq. Eng.*, vol. 55, no. 2, 2022, doi: 10.5459/BNZSEE.55.2.64-79.

[23] H. W. Shenton III, "Criteria for initiation of slide, rock, and slide-rock rigid-body modes," *J. Eng. Mech.*, vol. 122, no. 7, pp. 690–693, 1996.

[24] G. W. Housner, "The behavior of inverted pendulum structures during earthquakes," *Bull. Seismol. Soc. Am.*, vol. 53, no. 2, pp. 403–417, 1963.

[25] N. Makris and Y. S. Roussos, "Rocking response of rigid blocks under near-source ground motions," *Géotechnique*, vol. 50, no. 3, pp. 243–262, 2000.

[26] N. M. Newmark, "Effects of earthquakes on dams and embankments," *Géotechnique*, vol. 15, no. 2, pp. 139–160, 1965.

[27] W. A. Ghafar, T. Zhong, Z. Lai, Z. Pingle, Y. Yang, and M. M. Hasan, "Seismic isolation for existing structures: a review of retrofitting techniques, case studies, and trends," *Discov. Civ. Eng.*, vol. 2, no. 1, 2025, doi: 10.1007/s44290-025-00300-1.

[28] M. A. Q. Al-Janabi, D. Al-Jeznawi, T. Y. Yang, L. F. A. Bernardo, and J. M. de A. Andrade, "Enhancing structural resilience for sustainable infrastructure: a global review of seismic isolation and energy dissipation practices," *Sustainability*, vol. 17, 2025, doi: 10.3390/su17167314.

[29] S. Meerow, J. P. Newell, and M. Stults, "Defining urban resilience: a review," *Landsc. Urban Plan.*, vol. 147, pp. 38–49, 2016, doi: 10.1016/j.landurbplan.2015.11.011.

[30] G. Datola, "Implementing urban resilience in urban planning: a comprehensive framework for urban resilience evaluation," *Sustain. Cities Soc.*, 2023, doi: 10.1016/j.scs.2023.104821.

[31] T. Gu, J. Hu, X. Song, H. Yan, and Z. Chen, "How to enhance the urban community resilience from the perspective of social networks? A case study of Xuzhou, China," *Eng. Constr. Archit. Manag.*, 2025, doi: 10.1108/ECAM-01-2025-0078.

[32] ASCE/SEI 7-22, *Minimum Design Loads and Associated Criteria for Buildings and Other Structures*. Reston, VA: American Society of Civil Engineers, 2022.

[33] EN 1993-1-8, *Eurocode 3: Design of steel structures — Part 1-8: Design of joints*. Brussels: CEN, 2005.

[34] Saudi Building Code National Committee, *Saudi Building Code (SBC 301, Loads and Forces)*. Riyadh: SBC National Committee. [Online]. Available: https:*www.sbc.gov.sa/En/Pages/default.aspx*

[35] International Code Council, *2021 International Building Code*. Country Club Hills, IL: ICC, 2020.

[36] M. C. Constantinou, A. Mokha, and A. Reinhorn, "Teflon bearings in base isolation II: Modeling," *J. Struct. Eng.*, vol. 116, no. 2, pp. 455–474, 1990.

[37] H. Olsson, K. J. Åström, C. Canudas de Wit, M. Gäfvert, and P. Lischinsky, "Friction models and friction compensation," *Eur. J. Control*, vol. 4, no. 3, pp. 176–195, 1998.

[38] P. R. Dahl, "A solid friction model," The Aerospace Corporation, El Segundo, CA, Tech. Rep. TOR-0158(3107-18)-1, 1968.

[39] COMSOL Multiphysics®, version 5.6, *Reference Manual: Global ODEs and DAEs; Time-Dependent Solver*. Stockholm, Sweden: COMSOL AB, 2020.

[40] ISO 10137:2007, *Bases for design of structures — Serviceability of buildings and walkways against vibrations*. Geneva: International Organization for Standardization, 2007.

[41] S. Mani, G. Karunasena, A. Hasan, and M. R. Hosseini, "What to assess in circular buildings: key performance indicators for circular transformation," *Smart Sustain. Built Environ.*, pp. 1–23, Mar. 2026, doi: 10.1108/SASBE-11-2025-0708.

[42] B. Güngör *et al.*, "Circularity tools and frameworks for new buildings," in *Springer Tracts in Civil Engineering*, 2025, doi: 10.1007/978-3-031-73490-8_16.

[43] F. Pomponi and A. Moncaster, "Circular economy for the built environment: a research framework," *J. Clean. Prod.*, vol. 143, 2017, doi: 10.1016/j.jclepro.2016.12.055.

[44] L. A. Akanbi *et al.*, "Salvaging building materials in a circular economy: a BIM-based whole-life performance estimator," *Resour. Conserv. Recycl.*, vol. 129, 2018, doi: 10.1016/j.resconrec.2017.10.026.

[45] B. Tozan, E. Hoxha, E. B. Stapel, and H. Birgisdóttir, "Prioritizing low-carbon materials and reducing material quantities to mitigate embodied GHG emissions in buildings," *Sustain. Cities Soc.*, vol. 131, 2025, doi: 10.1016/j.scs.2025.106770.

[46] J. Wei, B. Ge, Y. Zhong, T. L. Lee, and Y. Zhang, "Comparative analysis of embodied carbon in modular and conventional construction methods in Hong Kong," *Sci. Rep.*, vol. 14, no. 1, 2024, doi: 10.1038/s41598-024-73906-7.

[47] W. Pan and Z. Zhang, "Benchmarking the sustainability of concrete and steel modular construction for buildings in urban development," *Sustain. Cities Soc.*, vol. 90, 2023, doi: 10.1016/j.scs.2023.104400.

[48] X. Wen, W. Pan, Y. Teng, D. W. M. Chan, and J. Xu, "Reducing or transferring emissions? Quantifying city-scale embodied carbon flows and emission responsibility in the modular construction supply chain," *Sustain. Cities Soc.*, vol. 145, p. 107470, Aug. 2026, doi: 10.1016/J.SCS.2026.107470.

[49] K. Belkhiri, A. Mitache, and V. Ungureanu, "Advancing circular economy strategies in modular architecture through design for disassembly and reuse," *Inżynieria Miner.*, vol. 2, no. 2, 2025, doi: 10.29227/IM-2025-02-02-021.

[50] C. Miller, "Sustainable shoring," in *Proc. Deep Foundations Institute 50th Annual Conf.*, Oct. 2025, doi: 10.37308/dfi50.1140804.

[51] N. Falah, N. Falah, J. Solis-Guzman, and M. Marrero, "An indicator-based framework of circular cities focused on sustainability dimensions and sustainable development goal 11 obtained using machine learning and text analytics," *Sustain. Cities Soc.*, vol. 121, 2025, doi: 10.1016/j.scs.2025.106219.

[52] A. Madanipour, "Temporary use of space: urban processes between flexibility, opportunity and precarity," *Urban Stud.*, vol. 55, no. 5, 2018, doi: 10.1177/0042098017705546.

[53] P. Bishop and L. Williams, *The Temporary City*. Abingdon: Routledge, 2012.

[54] M. Lydon and A. Garcia, *Tactical Urbanism: Short-term Action for Long-term Change*. Washington, DC: Island Press, 2015, doi: 10.5822/978-1-61091-567-0.

[55] J. Németh and J. Langhorst, "Rethinking urban transformation: temporary uses for vacant land," *Cities*, vol. 40, 2014, doi: 10.1016/j.cities.2013.04.007.

[56] J. Henneberry, *Transience and Permanence in Urban Development*. Chichester: Wiley-Blackwell, 2017, doi: 10.1002/9781119055662.

[57] G. Bertino, G. Rose, and J. Kisser, "Drivers and barriers for implementation and international transferability of sustainable pop-up living systems," *Circ. Econ. Sustain.*, vol. 1, no. 3, 2021, doi: 10.1007/s43615-021-00063-8.